Sensor and Simulation Notes

Note 401

October 1996

Development of a Reflector IRA and a Solid Dielectric Lens IRA Part II: Antenna Measurements and Signal Processing

Everett G. Farr
Farr Research, Inc.

Charles A. Frost
Pulse Power Physics, Inc.

Abstract

An earlier report (Sensor and Simulation Note 396) described the design and predictions for two reflector and lens Impulse Radiating Antennas (IRAs), with 23 centimeter diameters. In this note we complete the measurements of those antennas, and the data is processed and compared to theory. Antenna measurements were obtained using the two-antenna technique. Using signal processing, we extracted the one-way antenna response. The boresight step response in transmission (impulse response in reception) was measured to be as fast as 25 ps, Full Width Half Max (FWHM) for the reflector IRA, and 21 ps for the lens IRA. The impulse response on boresight for the reflector antenna has an impulse area of 87 % of the theoretically predicted value, and that for the lens is 101 % of the predicted value. The angular dependence of the antennas was measured, and the half-power points for both antenna types occurred approximately four degrees off-axis for step-function excitation. The dielectric-filled lens antenna, while heavier, showed higher performance than the reflector IRA.

This paper is a continuation of Sensor and Simulation Note 396, so it will be necessary to have it in hand to understand the ideas presented here.

CLEARED FOR PUBLIC RELEASE
AFDTC/PA 96-451
20 SEP 96

DEPARTMENT OF THE AIR FORCE
HEADQUARTERS AIR FORCE DEVELOPMENT TEST CENTER (AFMC)
EGLIN AIR FORCE BASE, FLORIDA

20 September 1996

MEMORANDUM FOR WL/CA-N
ATTN: DR. KWANG MIN

FROM: AFDTC/PA

SUBJECT: Clearance for Public Release

The technical note "Development of a Reflector IRA and a Solid Dielectric Lens IRA Part II: Antenna Measurements and Signal Processing" has been reviewed. Public release is approved.

Jim I. Swinson Jr

JIM I. SWINSON JR
Security & Policy Review Officer
Office of Public Affairs

SSN 401

Atch:
Tech Note

AFDTC/PA 96-451

Table of Contents

I. Introduction

A set of two reflector Impulse Radiating Antennas (IRAs) and two dielectric-filled lens IRAs have been fabricated according to the designs provided in [1]. The theory of both antenna types is reviewed, as are the time domain antenna equations. Measurements of the radiated fields in the E-plane and H-plane for both antenna types were performed. Furthermore, the impulse responses of the antennas were determined, and the gains were calculated as a function of angle. The beamwidth of the antennas was measured. The TDR of both antenna types was performed, and in the case of the reflector IRA, we verified the distance required to be in the far field by checking where the field started to depart from $1/r$ dependence..

Let us begin now with the theory of the Reflector IRA.

II. Reflector IRA Theory

Two identical reflector IRAs were built for this effort as described in [1]. Each antenna consisted of a 23 centimeter (9 in) diameter paraboloidal reflector with $F/D = 0.38$, fed by four triangular plates forming a conical TEM transmission line with a 200 Ω impedance. In this section we describe experiments used to characterize the reflectors, and we present the results. A diagram of the antenna was shown previously in Figures 2.B.1 through 2.B.3 of [1].

We begin by expressing the radiated field in transmission, and the received field in reception. For an ideal antenna with a single pair of arms, theory [2] predicts

$$E_{rad}(t) = \frac{a}{2\pi r c f_{g1}} \frac{dV_{inc}^{(arms)}(t)}{dt} \tag{2.1}$$

where a is the reflector radius, r is the observation point on boresight, c is the speed of light in free space, and f_{g1} is the normalized impedance across a single pair of arms, which is typically 400 Ω / 376.727 Ω. Furthermore, $V_{inc}^{(arms)}(t)$ is the incident voltage across the single pair of arms. If there are two pairs of arms with the same voltage across them, the above equation is modified to

$$E_{rad}(t) = \frac{(a/\sqrt{2})}{2\pi r c f_{g2}} \frac{dV_{inc}^{(arms)}(t)}{dt} \tag{2.2}$$

where f_{g2} is the normalized impedance for the four-arm structure with two pairs of arms, typically 200 Ω / 376.727 Ω. Finally, since there is some impedance mismatch between the input 50 Ω feed cable and the feed arms, we have

$$E_{rad}(t) = \frac{\tau_{t1}(a/\sqrt{2})}{2\pi r c f_{g2}} \frac{dV_{inc}^{(cable)}(t)}{dt} \tag{2.3}$$

where τ_{t1} is the ratio of the voltage on the feed arms to the voltage on the feed cable, and $V_{inc}^{(cable)}(t)$ is the incident voltage on the feed cable. Let us express this as

$$\begin{aligned} E_{rad}(t) &= \frac{\tau_{t1}}{2\pi r c f_{g2}} h(t) \circ \frac{dV_{inc}^{(cable)}(t)}{dt} \\ h(t) &= \frac{a}{\sqrt{2}} \delta(t) \end{aligned} \tag{2.4}$$

where $\delta(t)$ is the Dirac delta function and " ∘ " indicated a convolution. This is the final result we need to describe the antenna's behavior on boresight in transmission.

In reception, the received voltage across a single pair of feed arms is

$$V_{rec}^{(arms)}(t) = a\, E_{inc}(t) \tag{2.5}$$

With two pairs of arms, this becomes

$$V_{rec}^{(arms)}(t) = \frac{a}{\sqrt{2}} E_{inc}(t) \tag{2.6}$$

Furthermore, this is modified by the transmission coefficient from the arms to the cables, to obtain

$$V_{rec}^{(cable)}(t) = \frac{\tau_{t2}\, a}{\sqrt{2}} E_{inc}(t) \tag{2.7}$$

where τ_{t2} is the ratio of the voltage excited on the feed arms to the voltage in the 50 Ω cable. Using the same $h(t)$ which was used previously in (2.4), we have

$$\begin{aligned} V_{rec}^{(cable)}(t) &= \tau_{t2}\, h(t) \circ E_{inc}(t) \\ h(t) &= \frac{a}{\sqrt{2}} \delta(t) \end{aligned} \tag{2.8}$$

Finally, we expand the above $h(t)$ to include the prepulse [2], so

$$h(t) = \frac{a}{\sqrt{2}} \left[\delta(t - 2F/c) - \frac{c}{2F} [u(t) - u(t - 2F/c)] \right] \tag{2.9}$$

This is the characteristic function of the antenna which we will measure.

Using the two-antenna method, we will measure on boresight

$$V_{rec}^{(cable)}(t) = \frac{\tau_{t1}\, \tau_{t2}}{2\pi r c f_{g2}} h(t) \circ h(t) \circ \frac{d\, V_{inc}^{(cable)}}{dt} \tag{2.10}$$

Thus, in the experiment we can use the measured cable voltages to extract $h(t)$, the boresight response. When we scan in the E- or H-plane, we have to modify one of the $h(t)$s to indicate a response off-boresight. Thus, we measure

$$V_{rec}^{(cable)}(t) = \frac{\tau_{t1}\, \tau_{t2}}{2\pi r c f_{g2}} h(t) \circ h^{(e)}(t,\theta) \circ \frac{d\, V_{inc}^{(cable)}}{dt} \tag{2.11}$$

in the E-plane, where $h^{(e)}(\theta, t)$ is the antenna characteristic as a function of angle θ off boresight in the E-plane. An analogous expression using $h^{(h)}(\theta,t)$ is true in the H-plane.

We have not yet calculated the transmission coefficients, so let us do so now. There is a 75 Ω transmission line transformer cable that lies between the 50 Ω feed cable and the 200 Ω input impedance to the antenna. Note that we did not use the double-gap design using two 100 Ω cables, as proposed in [1] and as described originally by Baum in [3]. Better performance was observed with the single 75 Ω feed, as described in the next paragraph. In general, the transmission coefficient at a transmission line discontinuity is

$$\tau = \frac{2Z_2}{Z_1 + Z_2} \tag{2.12}$$

where Z_1 is the impedance of the incident line and Z_2 is the impedance of the transmit line. For transmission, we have discontinuities from 50 Ω to 75 Ω, and again from 75 Ω to 200 Ω. For reception, we have discontinuities from 200 Ω to 75 Ω, and from 75 Ω to 50 Ω. Thus, the total transmission coefficients for transmission and reception are

$$\begin{aligned} \tau_{t1} &= \frac{2\times75}{50+75}\times\frac{2\times200}{75+200} = 1.745 \\ \tau_{t2} &= \frac{2\times75}{200+75}\times\frac{2\times50}{75+50} = 0.436 \\ \tau_{t1}\times\tau_{t2} &= 0.76 \end{aligned} \tag{2.13}$$

Thus, we see that the absolute magnitude of the received voltage is reduced by a factor of 0.76 because of the impedance discontinuities in transmission and reception.

It is reasonable to ask why this loss was tolerated, since the splitter balun [3] seems to avoid all discontinuities, at least at low frequencies. There are several reasons. First, the 100 Ω cable which we would have used has a very thin center conductor, which is fragile and breaks easily. Second, the balun suggested by Baum has a double gap at the apex, instead of the single gap used in our antenna. This double gap is necessarily larger than a single gap, so the structure has reduced high-frequency performance, which was apparent as a slower risetime. Since the radiated field was proportional to *dV/dt*, it was important not only to avoid discontinuities, but also to avoid any slowdown in the risetime of the antenna. Measurements were conducted with both designs, using a single antenna with a reflecting plate in a TDR configuration. It was found that the single 75 Ω cable transformer design provided the largest received voltage after reflection from the plate. We assume this is because the impedance mismatch was less important than the preservation of the high-frequency response. For this reason, we used the single 75 Ω cable, instead of the design proposed by Baum in [3].

III. Experimental Setup for Reflector IRA

We summarize here the measurement system used to characterize the reflector IRAs. A technique was used in which one antenna always pointed on boresight, and one antenna scanned in the E- and H-planes. The method was described in detail in [1].

The method used here is preferable to that used in an earlier paper [2]. In that work we measured the antenna characteristic on boresight using a TDR-like technique, with a reflection from a metal plate [2]. While this method allows rapid optimization of the antennas, it suffers from late-time artifacts due to diffraction from the edge of the plate. For this reason, final antenna calibrations and pattern measurements were performed outdoors (to avoid reflections) on a wooden platform using two antennas. The method using two identical antennas was described in [1]. We have improved the measurement over what was originally proposed by upgrading to the PSPL4015C pulser, which has a remote pulse head providing 4V output with < 20 ps risetime and the Tektronix 11801 digital sampling oscilloscope with a terminated SD-20 sampler. The setup is shown in Figures 3.1 and 3.2. The 11801 was operated at 10 mV/div and 500 ps/div, and 5120 points were sampled on each scan. In order to eliminate interference from nearby radio and television transmitters, 4096 scans were averaged for each waveform.

The receiving antenna was coupled to the sampling head by a 0.91 meter (36 in) length instrumentation grade Goretex SMA port cable. To minimize ground bounce, the receiving antenna was located on a wooden platform at a height of 4.32 meters (170 in) above the surrounding terrain. The transmitting antenna and pulser were located at a height of 1.32 meters (52 in) above the ground, which sloped gently away from the platform. The remote pulse head was attached directly to the transmitting antenna without an intervening cable. The total path length of 6.63 meters (261 in) ensured far-field conditions. This arrangement caused the receive antenna to point down with a 30 degree angle with respect to the horizontal. As shown in Figure 3.2, the 30 degree inclination avoided a ground bounce, but it precluded a pure H-plane scan. For system calibration, the remote pulse head was connected to the input of the 0.91 meter (36 in) Gore-tex port cable through a type-K (40 GHz) 20 dB attenuator.

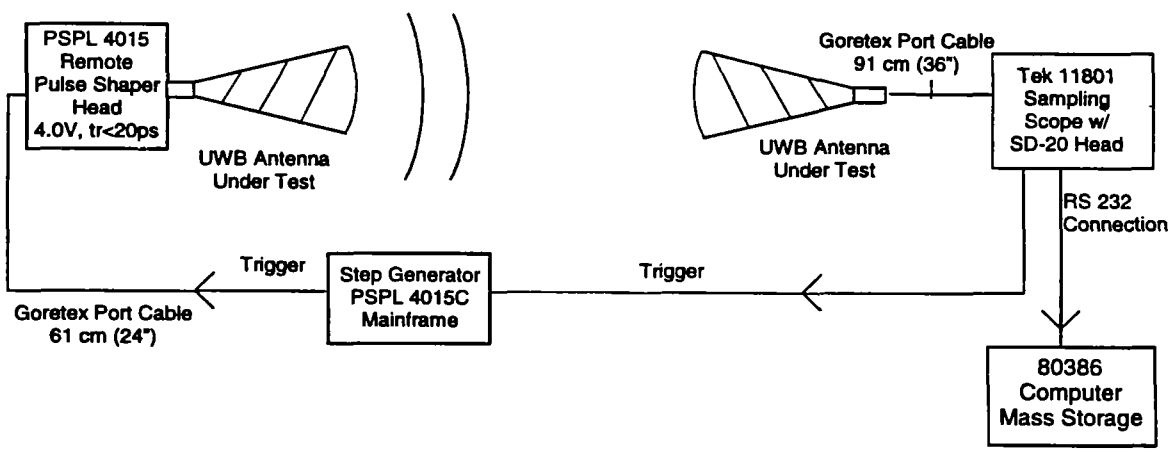

Figure 3.1. The experimental test configuration.

The antennas were separated by a distance of 6.629 meters (261"). The fiberglass feed arm supports were removed for the measurements to provide the fastest possible pulse. The supports are only used for shipping. The transmitting antenna was constantly pointed at the receiving antenna, which was scanned in either the E plane or (approximately) in the H-plane. The angles in both planes were measured to within an accuracy of plus or minus two degrees, using protractor scales on the azimuth-elevation mount. A minor limitation in our test configuration precluded a pure H-plane scan at 30 degree inclination. The azimuth-elevation mount we were using did not allow a true H-plane scan, but it allowed one 30 degrees below the horizon. We call this a "pseudo-H-plane" scan, and this is shown in Figure 3.2. The receiving antenna is scanned about a vertical axis, while pointed down at 30 degrees. This is a true H-plane near boresight, out perhaps to 10 degrees, with a bit higher error off boresight. The E-plane scan is unaffected by this perturbation.

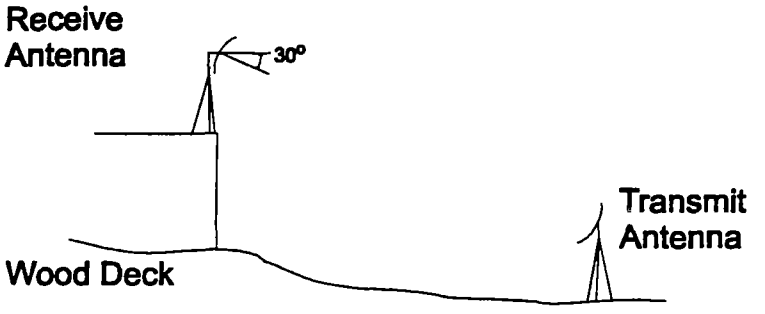

Figure 3.2. The arrangement of the two antennas. The receive antenna is rotated about a vertical axis during the pseudo H-plane scan. The receive antenna can rotate up and down for a true E-plane scan.

IV. Results for the Reflector IRA

During all the experiments, we excite the antenna with a step voltage, and measure the received voltage. To normalize our measurements, we connected the step generator to the sampling scope, using all the cabling that was used in the experiment. The 16.5 cm (6.5-in), 75 Ω transformer cables are part of the antenna, and so were left out of this normalization procedure. Note that all waveforms were taken as sets of 5120 points spaced 1 ps apart. Each waveform was then truncated to 4096 points, and the data set was reduced by a factor of two by averaging every two points, resulting in a waveform of 2048 points. Finally a dc offset was applied to force the waveform to begin at zero.

The step function normalization waveform is shown in Figure 4.1 (top). The derivative of the resulting waveform, after filtering with the modified Butterworth with $N = 10$ and $f_o = 30$ GHz is shown in Figure 4.1 (middle). The modified Butterworth filter is described by

$$G(f) = \frac{1}{1+(f/f_o)^{2N}} \tag{4.1}$$

Finally, a frequency spectrum of the waveform is shown on the bottom of Figure 4.1. This spectrum is for the complete measurement system response, including source, sampler, and cabling. It was necessary to include a 20 dB (factor of 10) attenuator in the loop, to avoid overdriving the sampling head. The plots in Figure 4.1 have been corrected for this attenuator. Thus, the measurement, including the attenuator (PSPL 5510-K-20) was a step function of about 0.4 V, but we plot the system waveform of 4 V, with the attenuator removed.

The received voltages for the E-plane are shown in Figure 4.2.(a), and a closeup of the peaks is shown in Figure 4.2(b). This is repeated for the pseudo H-plane data in Figures 4.2(c) and 4.2(d). These data sets have all been filtered in the frequency domain by the modified Butterworth filter, with $N = 10$ and f_o=30 GHz.

The frequency spectra for the E-plane and pseudo H-plane patterns are shown in Figures 4.3(a) and 4.3(b). It is interesting to note that the high frequencies are lost at the wider angles, as we would expect.

The next step is to normalize the waveforms to the derivative of the system response, as provided earlier in Figure 4.1(b). The normalized E-plane response is shown in Figures 4.4(a) and 4.4(b), and the normalized pseudo H-plane response is shown in Figures 4.4(c) and 4.4(d). These waveforms are what would be seen with a perfect step source and measurement system, with 6.63 meters (261 in.) of antenna separation. These waveforms are unitless, but if a one-volt step were used, it would show the output in volts.

From these waveforms we can measure the FWHM for the on- and off-boresight cases. The results are shown in Table 4.1. Note that the waveforms are assumed to begin at a level of −0.002. This corrects for a pedestal preceding the impulse that starts below zero. Finally, we

show the corrected spectra of the receive signal, as shown in Figures 4.5(a) and 4.5(b). Once again, we see that the high frequencies fall off sharply at wide angles.

Table 4.1. Pulse Widths of the Received Voltages as a Function of Angle, After Normalization.

	Angle (deg)	t_{FWHM} (ps)
E-Plane	0	33
	5	52
	10	85
H-Plane	0	33
	5	36
	10	59

Next, we extract the $h(t)$ for the antenna, which is the step response in transmission, or the impulse response in reception, as shown in Equation (2.10). This process was described in [2]. To do so, we obtained $H(f)^2$ in the frequency by multiplying the normalized received voltage by $2\pi rcf_{g2}/\tau_{t1}\tau_{t2}$, where f_{g2} = 200/376.727, and all the other parameters are defined near Equation (2.10). Furthermore, it was necessary to unwrap the phase by adding a time delay to $H(f)^2$ to bring the peak to time=0. After taking the square root, the resulting $H(f)$, with phase unwrapped, is shown in Figure 4.6. After converting to the time domain, and restoring the time delay, the boresight impulse response, $h(t)$ is shown in Figure 4.7.

Let us consider now some of the properties of the extracted $h(t)$. First, it is striking how closely the extracted $h(t)$ resembles our simple model of a step function, followed by an impulse function. Our measured $h(t)$ has a FWHM of 25 ps, which is quite fast by current standards. Note that the FWHM was measured from a baseline of –0.125 m/ns. Furthermore, the area under the impulse is 6.5 cm, also as measured from a baseline of –0.125 m/ns. Simple theory predicts this to be $a/\sqrt{2}$ = 8.1 cm. A more complete theory [4], which includes feed blockage, reduces the value of the simple theory by a factor of 0.92. Thus, our measurement is 6.5 cm / (0.92 × 8.5 cm) = 87 % of the impulse area predicted by our best theory.

With $h(t)$ derived, we can now extract the antenna pattern data. To do so, we multiply the normalized received voltages of Figure 4.4 by $2\pi rcf_{g2}/\tau_{t1}\tau_{t2}$, and divide in the frequency domain by the Fourier transform of $h(t)$, or $H(\omega)$. At this stage we applied an additional modified Butterworth filter with parameters N = 10 and f_o = 25 GHz. In addition, it was necessary to limit the zeroes of $H(f)$, to avoid dividing by a small number. We therefore limited $H(f)$ to be no smaller than H_{min}, where H_{min} = Max ($|H(f)|$) x 0.1, using

$$H_{\lim}(f) = \frac{H(f)}{|H(f)|}\sqrt{H_{\min}{}^2 + |H(f)|^2} \qquad (4.2)$$

Thus, instead of dividing by $H(f)$, we divided by $H_{lim}(f)$, to avoid oscillations in the final result. The frequency response is then converted to the time domain, giving $h(\theta, t)$ as defined by equation (2.11), and the results are shown in Figure 4.8 in the time domain and Figure 4.9 in the frequency domain.

A table of the FWHM of the recovered $h(t)$s is shown in Table 4.2. As expected, the FWHM increases with increasing angle off-boresight.

Table 4.2. Pulse Widths of the $h(\theta, t)$ as a Function of Angle.

	Angle (deg)	t_{FWHM} (ps)
E-Plane	0	25
	5	51
	10	89
H-Plane	0	25
	5	31
	10	61

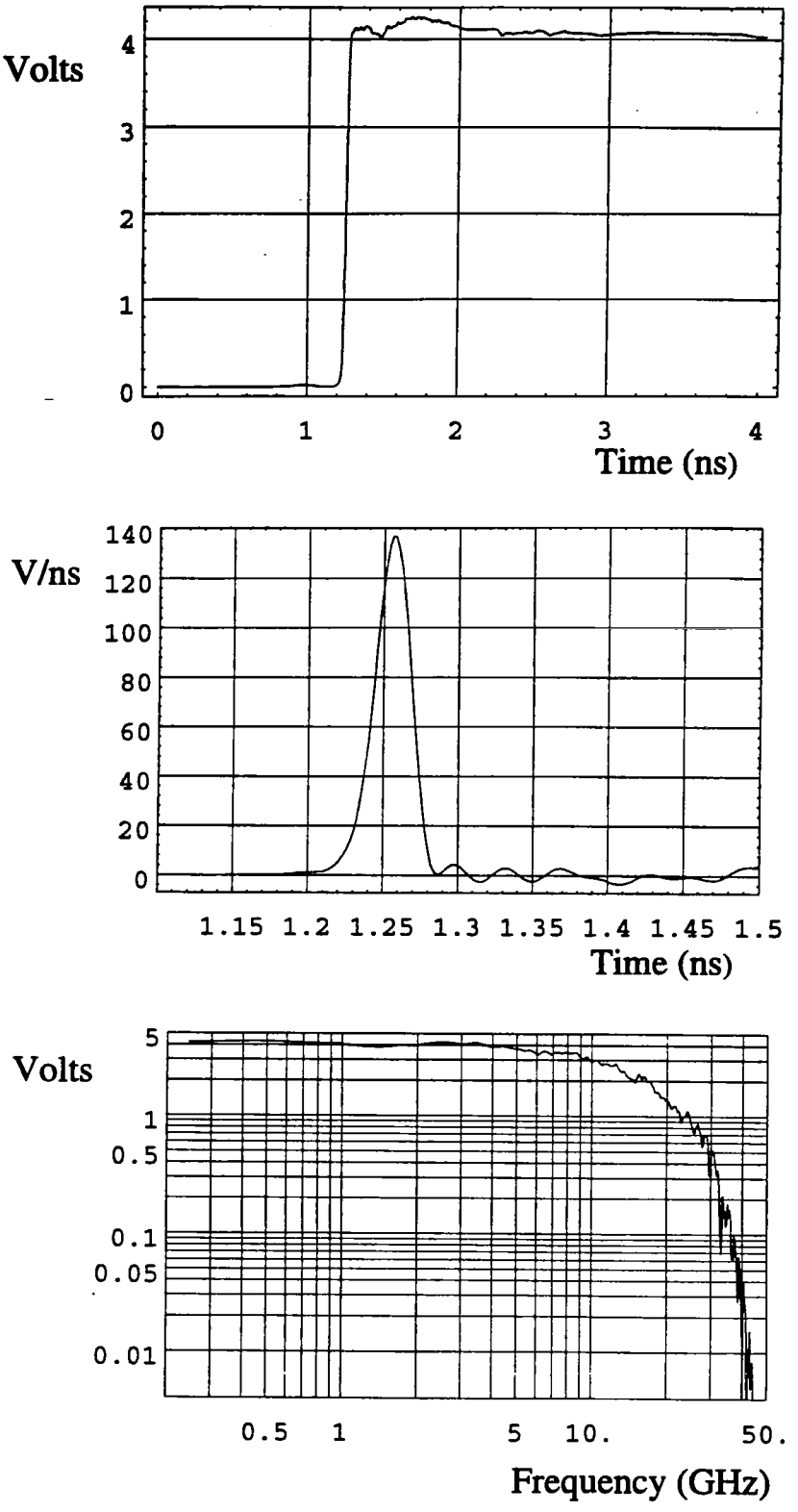

Figure 4.1. The system excitation response (incident voltage and cabling) (top), its derivative (middle) and its unfiltered frequency spectrum (bottom).

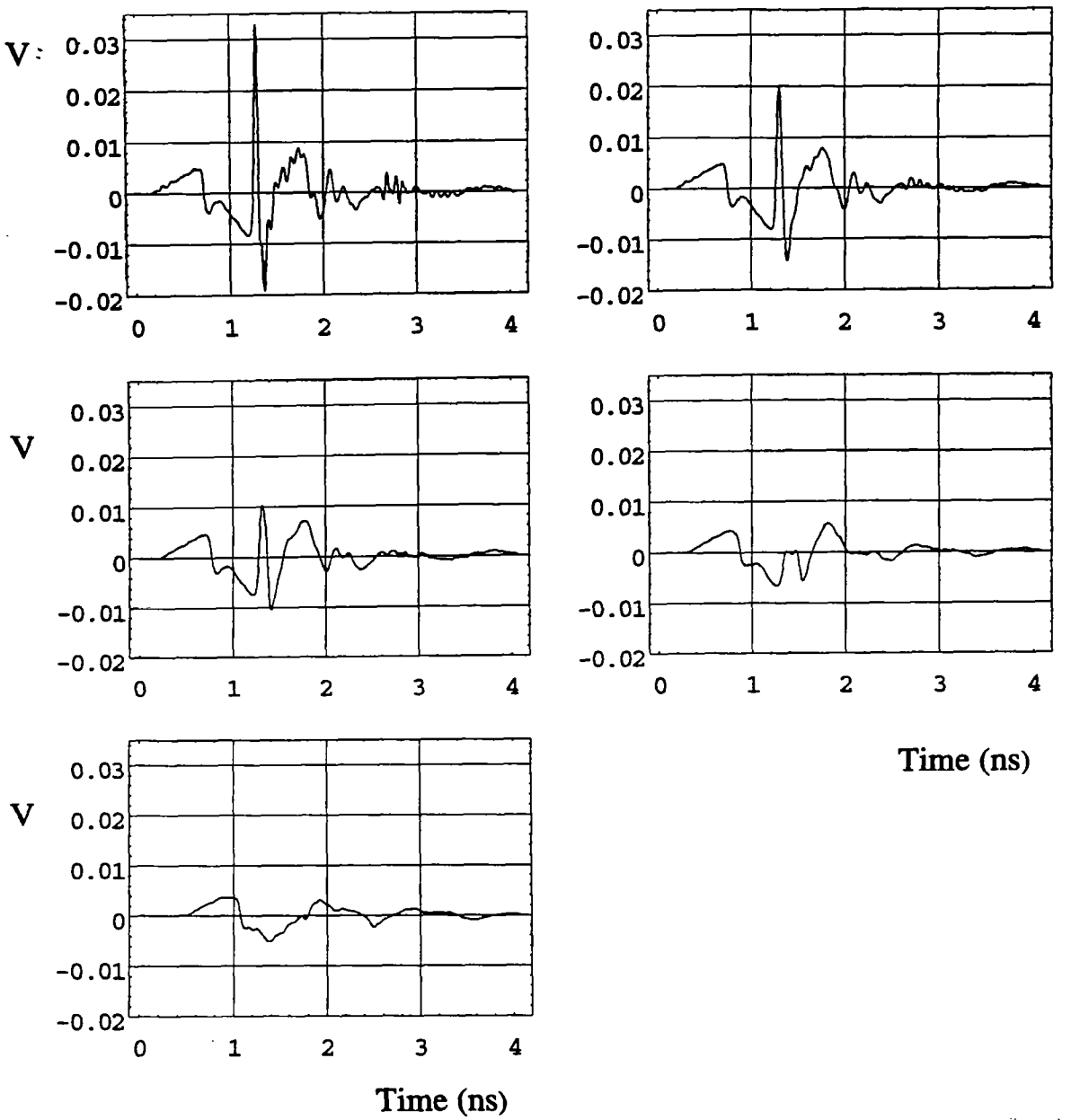

Figure 4.2(a). E-plane received voltage, after filtering. Waveforms are at 0, 5, 10, 20 and 40 degrees off boresight

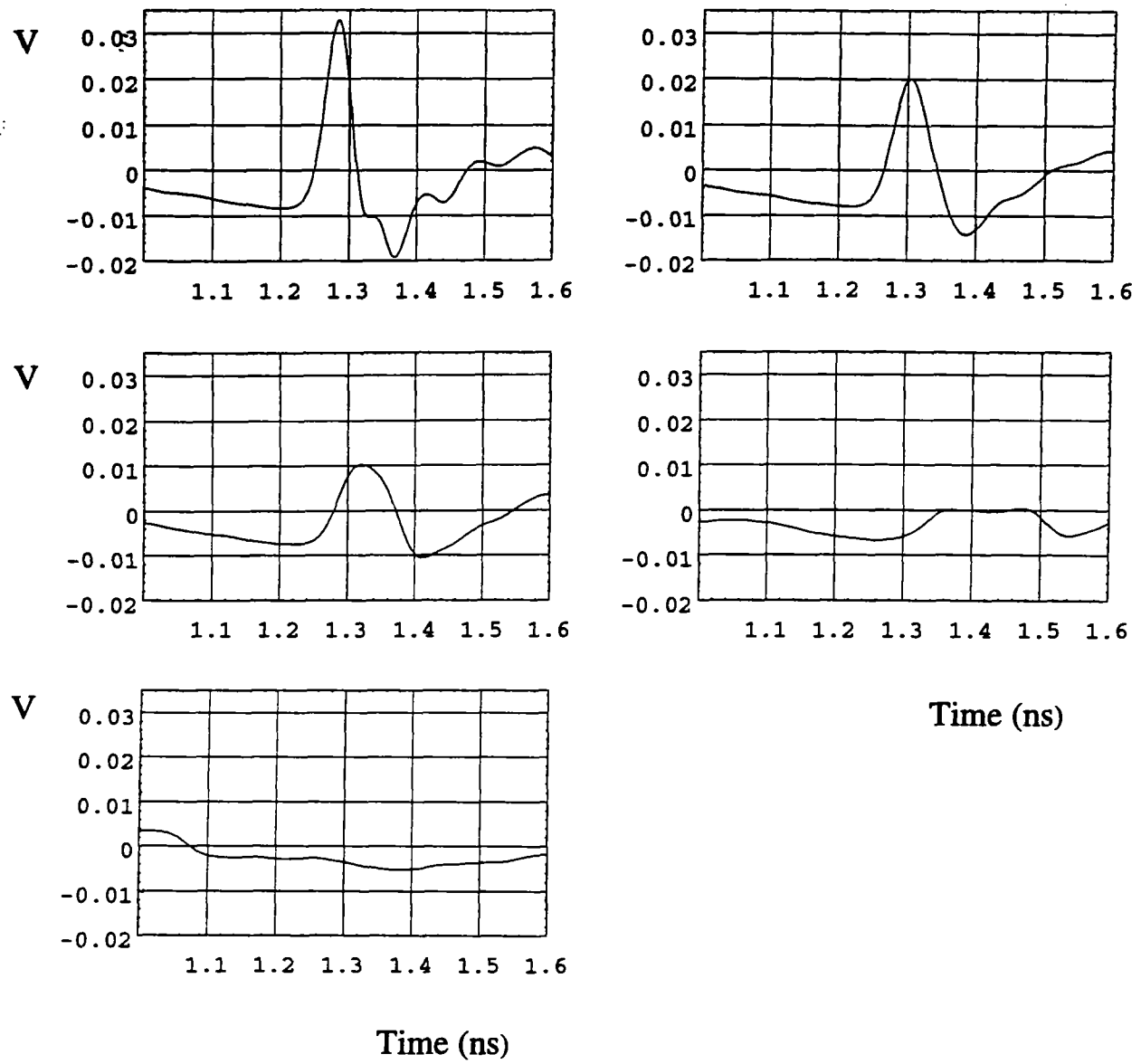

Figure 4.2(b). Closeup of the peaks in Figure 4.2(a).

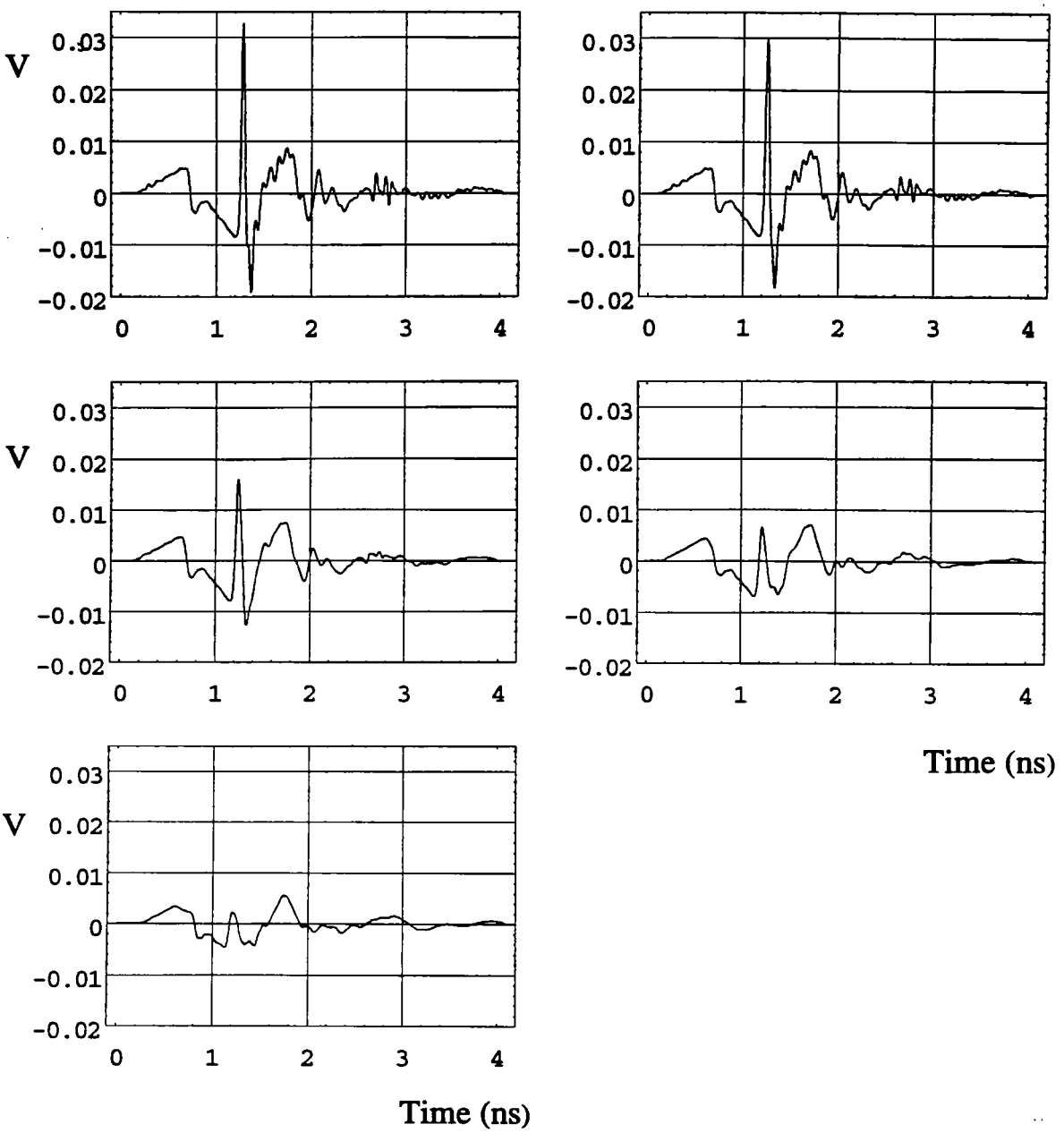

Figure 4.2(c). Pseudo H-plane received voltage, after filtering. Waveforms are at 0, 5, 10, 20 and 40 degrees off boresight

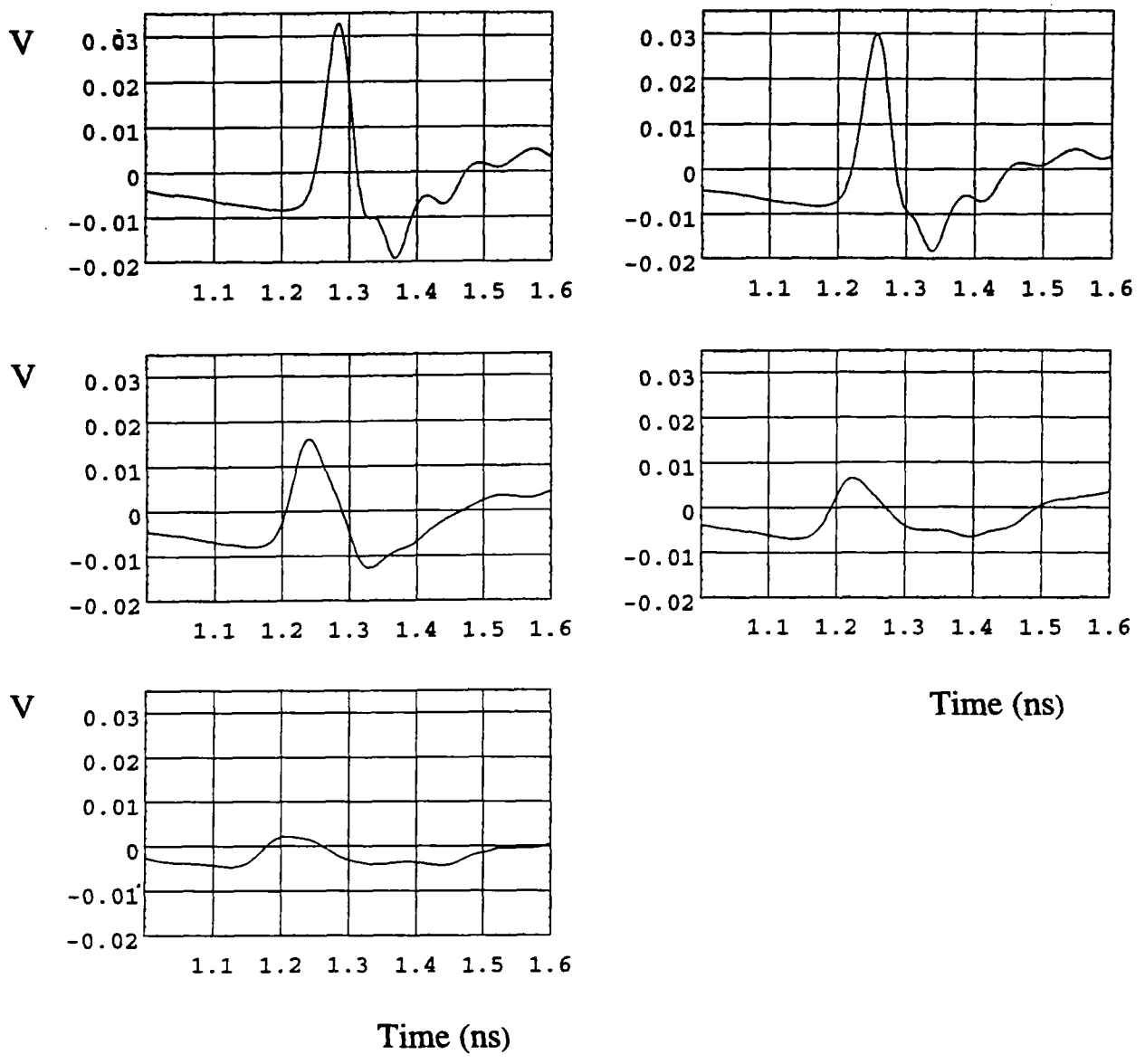

Figure 4.2(d). Closeup of the peaks in Figure 4.2(c).

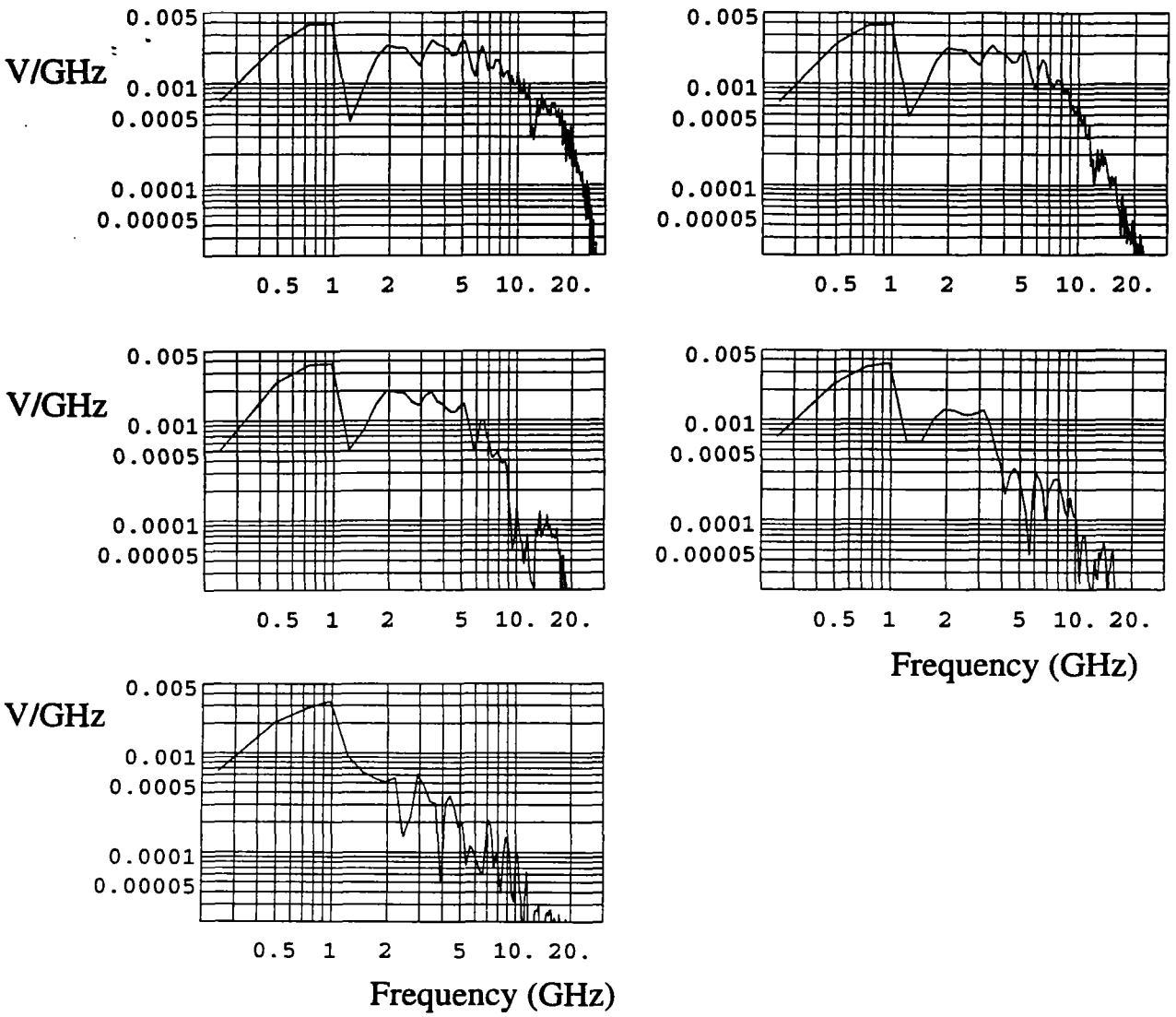

Figure 4.3(a). E-Plane scan, filtered but unnormalized, in the frequency domain. Waveforms are at 0, 5, 10, 20 and 40 degrees off boresight

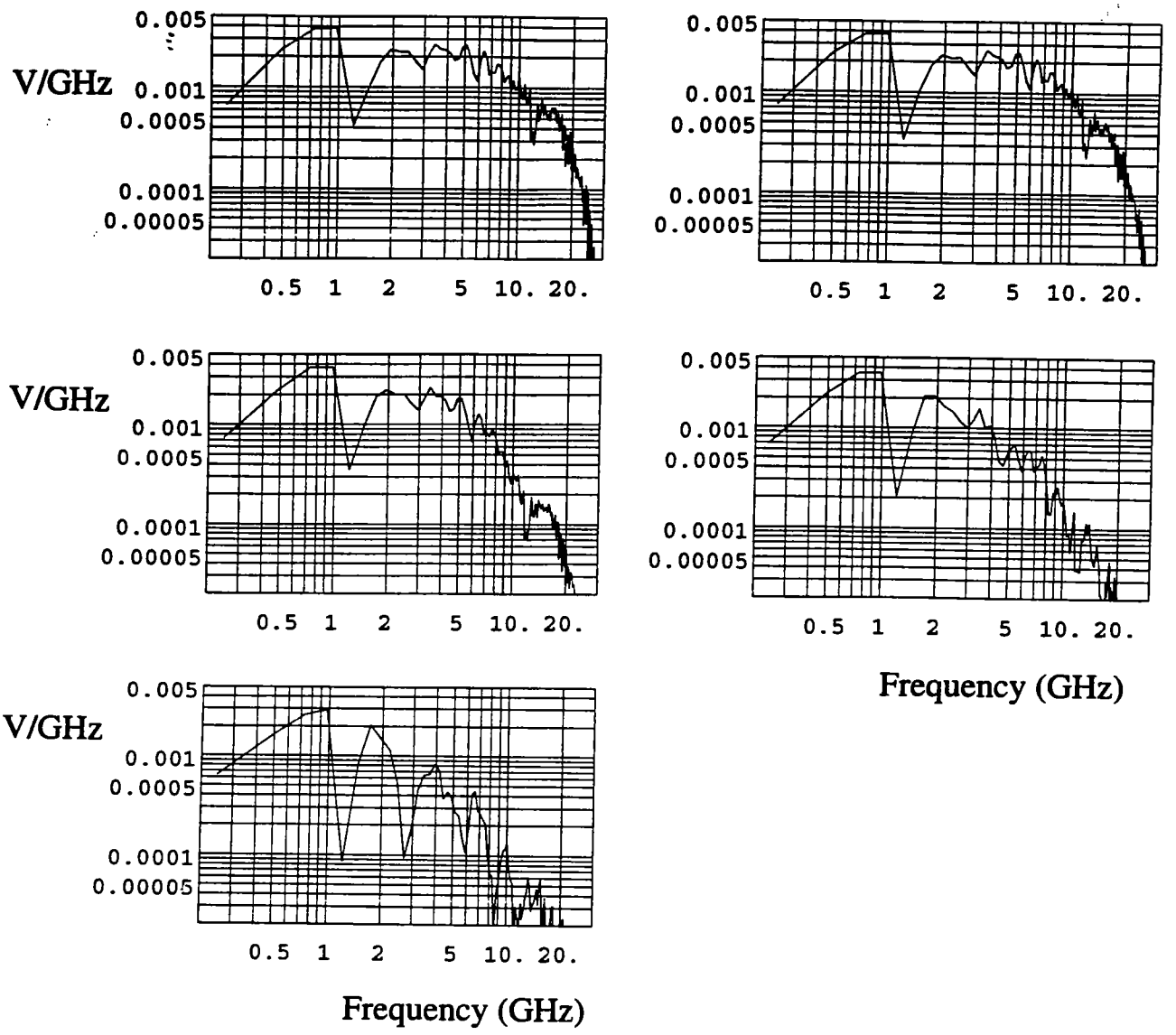

Figure 4.3(b). Pseudo H-Plane scan, filtered but unnormalized, in the frequency domain. Waveforms are at 0, 5, 10, 20 and 40 degrees off boresight

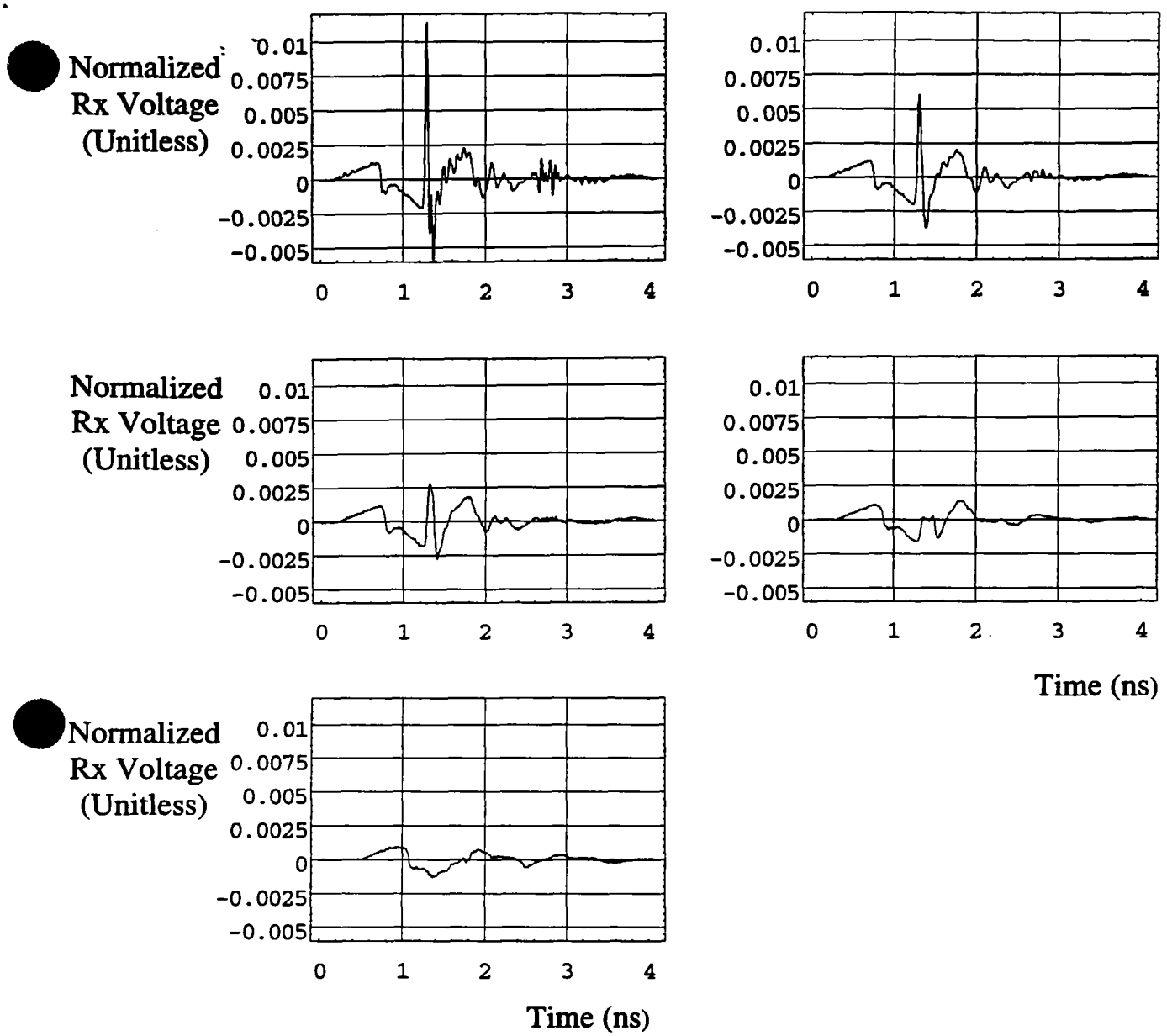

Figure 4.4 (a). E-plane received voltage, after filtering and normalization. Waveforms are at 0, 5, 10, 20 and 40 degrees off boresight.

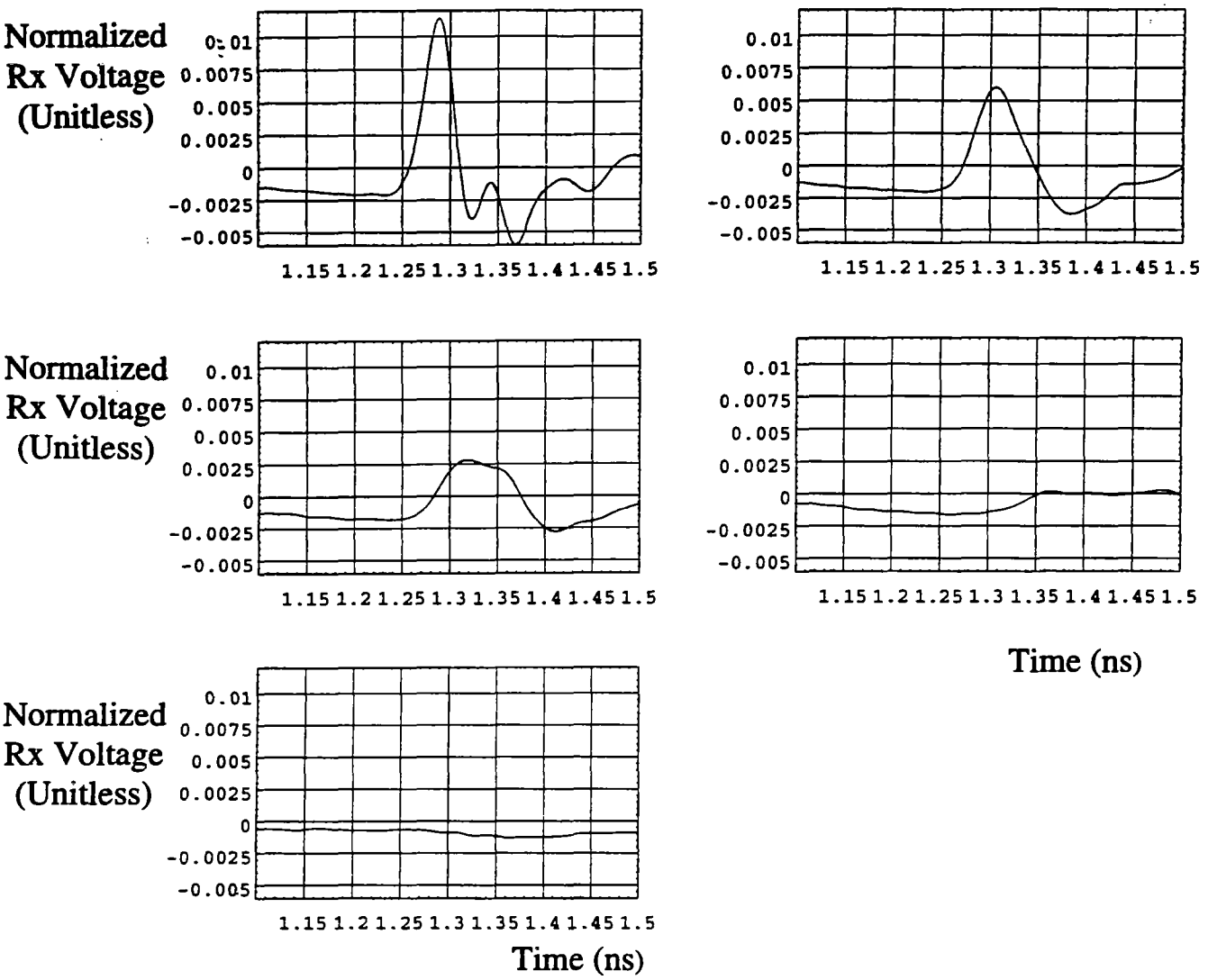

Figure 4.4 (b). Closeup of the peaks in Figure 4.4 (a).

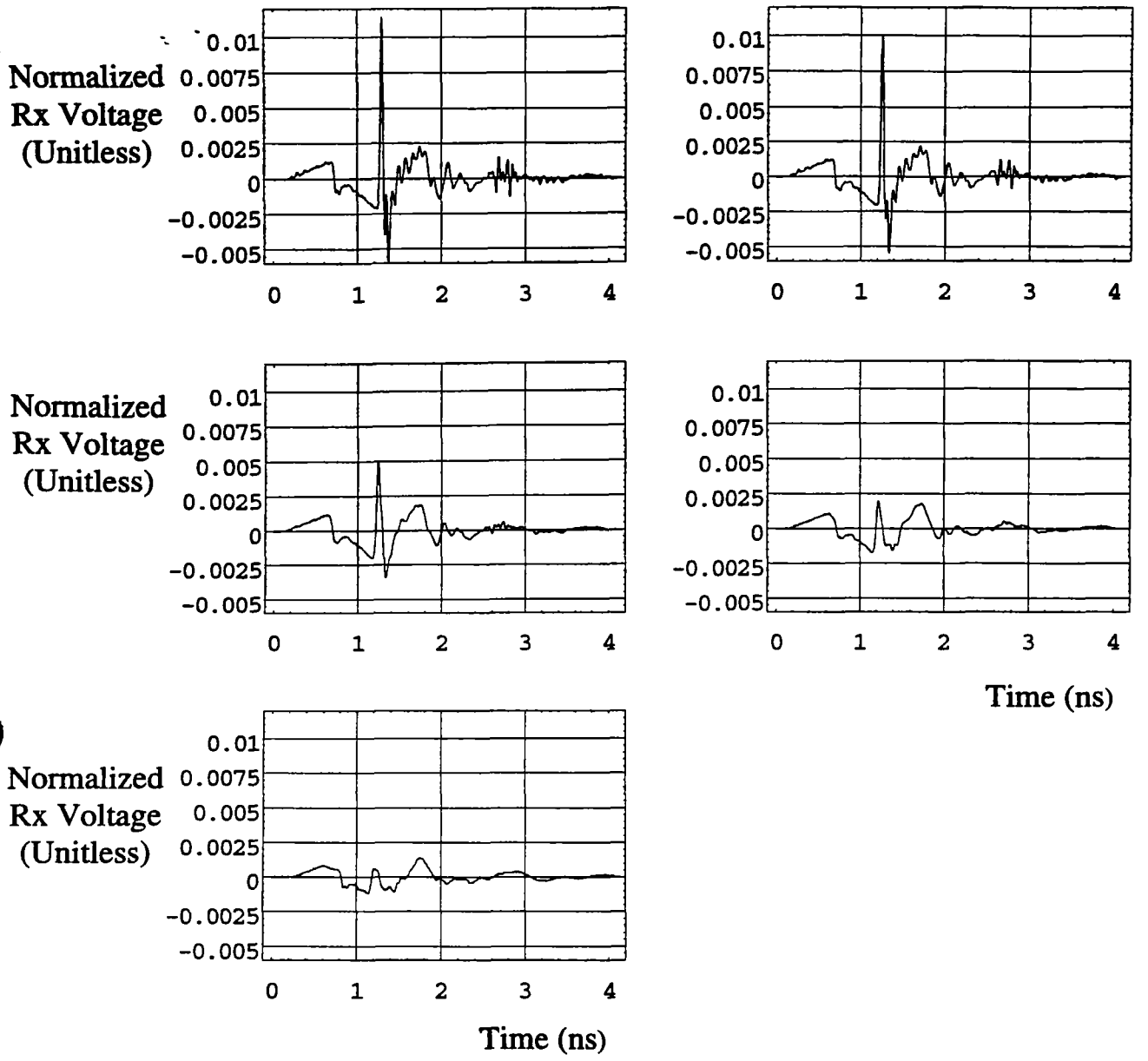

Figure 4.4 (c). Pseudo H-plane received voltage, after filtering and normalization. Waveforms are at 0, 5, 10, 20 and 40 degrees off boresight.

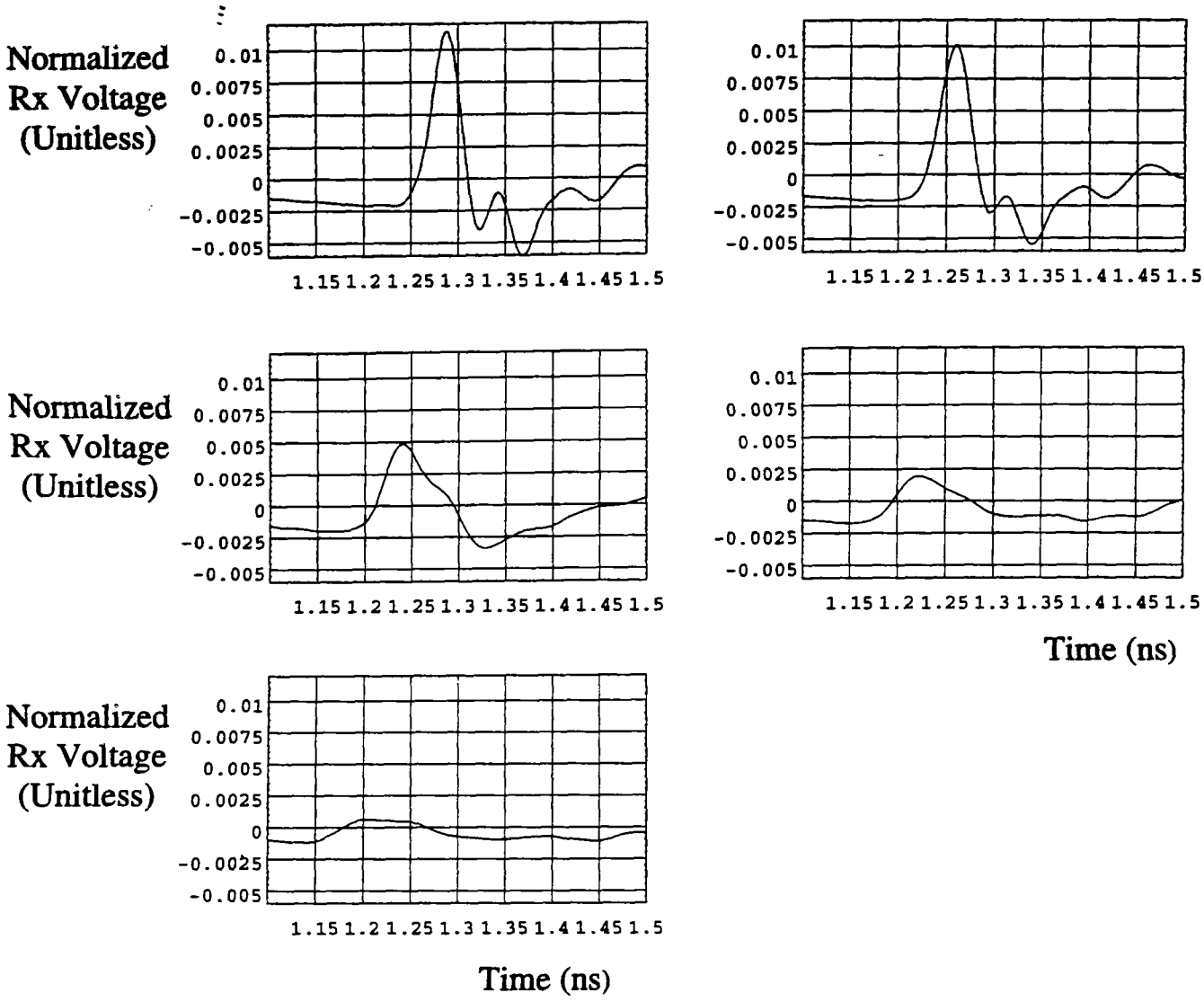

Figure 4.4 (d). Closeup of the peaks in Figure 4.4 (c).

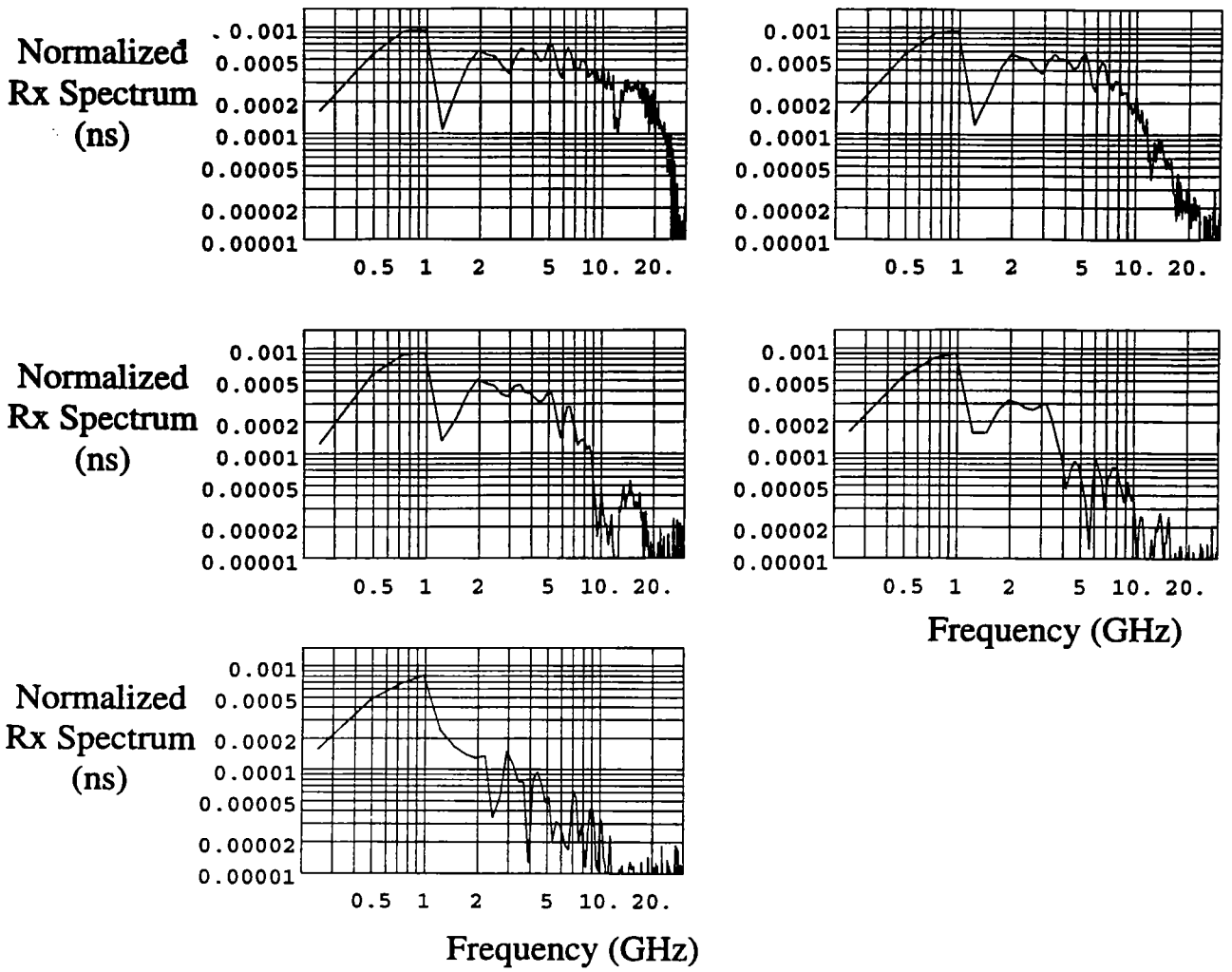

Figure 4.5 (a). E-Plane received voltage, after filtering and normalization, in the frequency domain. Waveforms are at 0, 5, 10, 20 and 40 degrees off boresight.

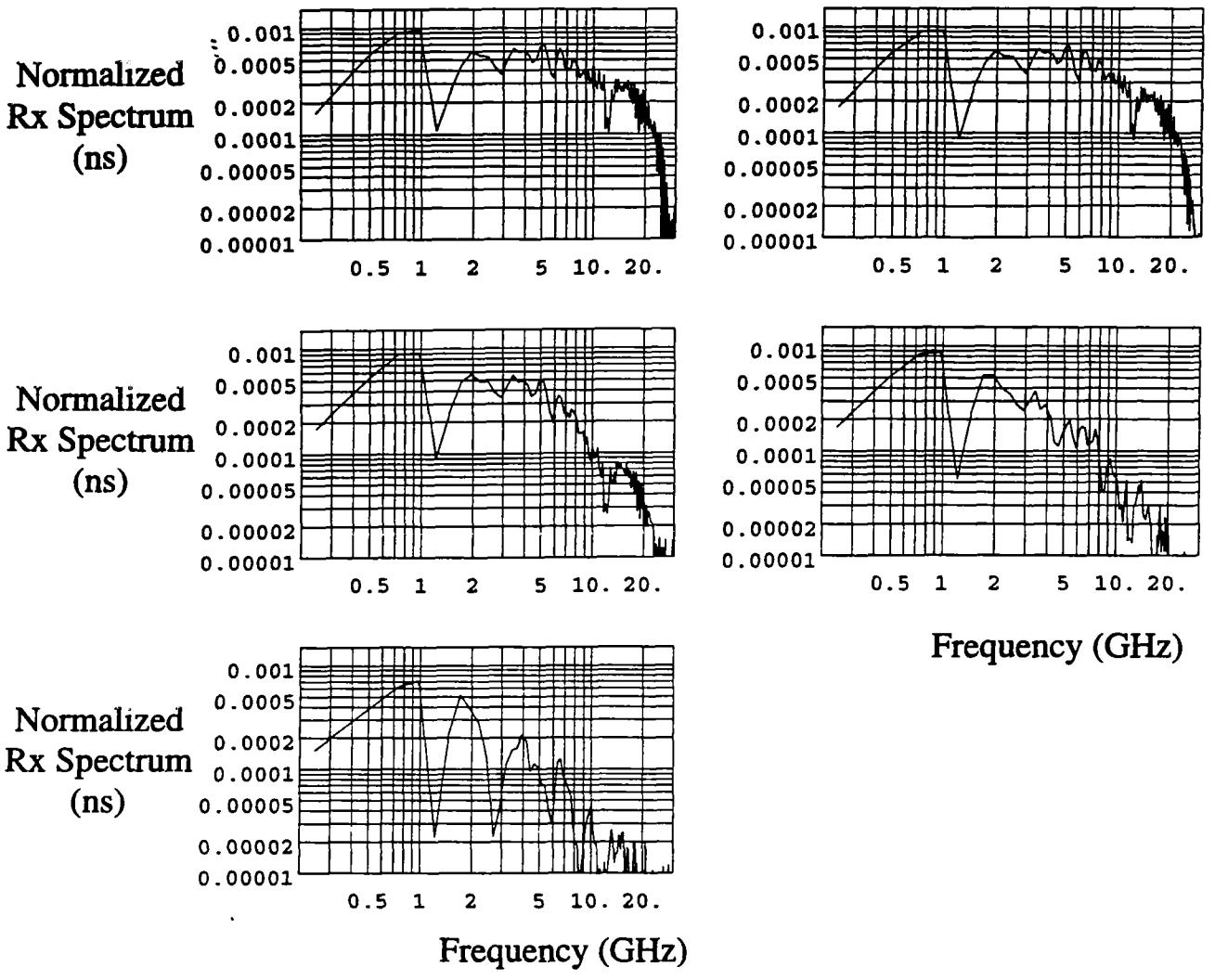

Figure 4.5 (b). Pseudo H-Plane received voltage, after filtering and normalization, in the frequency domain. Waveforms are at 0, 5, 10, 20 and 40 degrees off boresight.

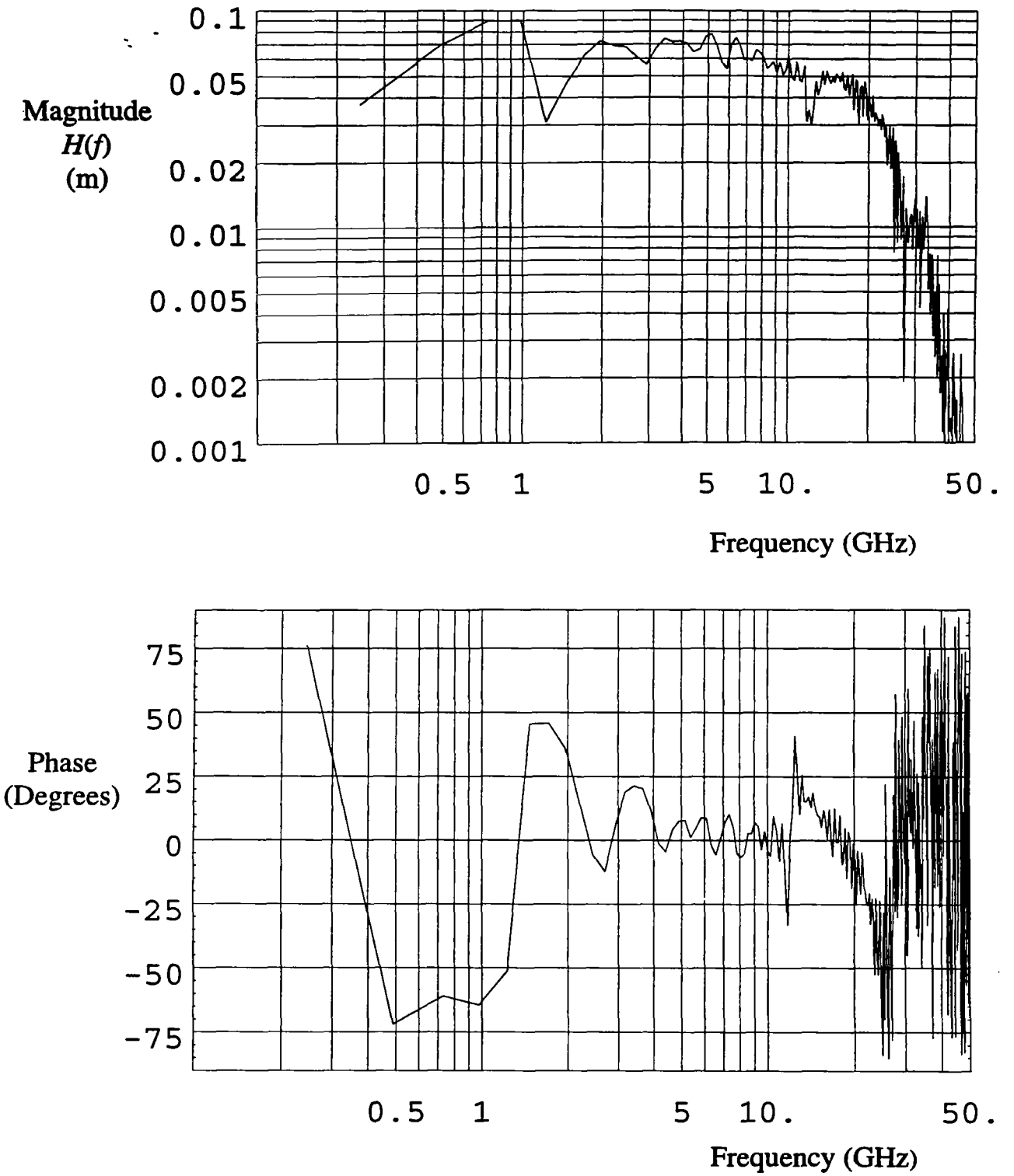

Figure 4.6. Frequency domain $H(f)$, just after taking the square root, magnitude (top) and phase (bottom). Note that the phase is essentially flat at the mid-band.

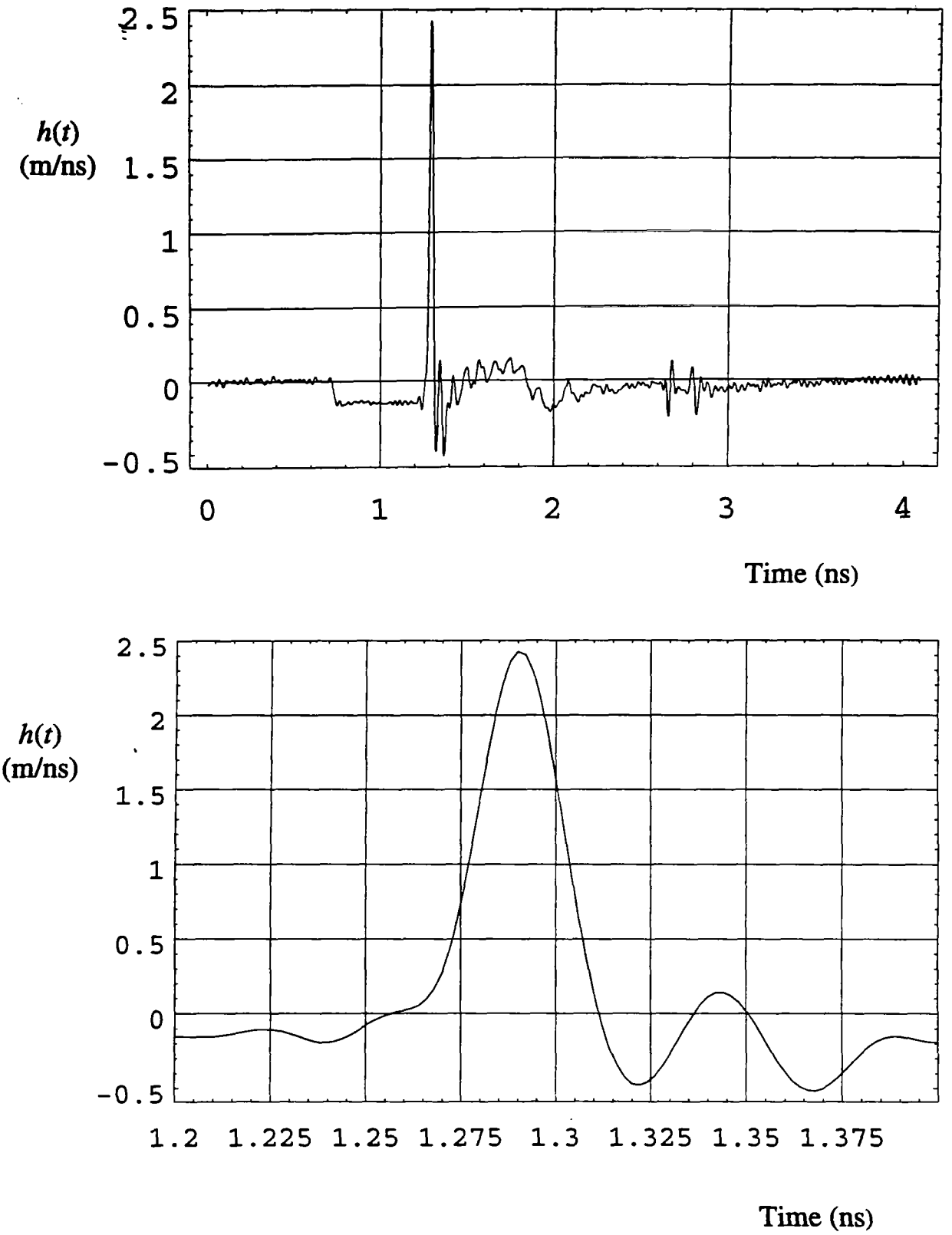

Figure 4.7 Boresight $h(t)$, entire waveform (top) and a closeup of the impulse (bottom).

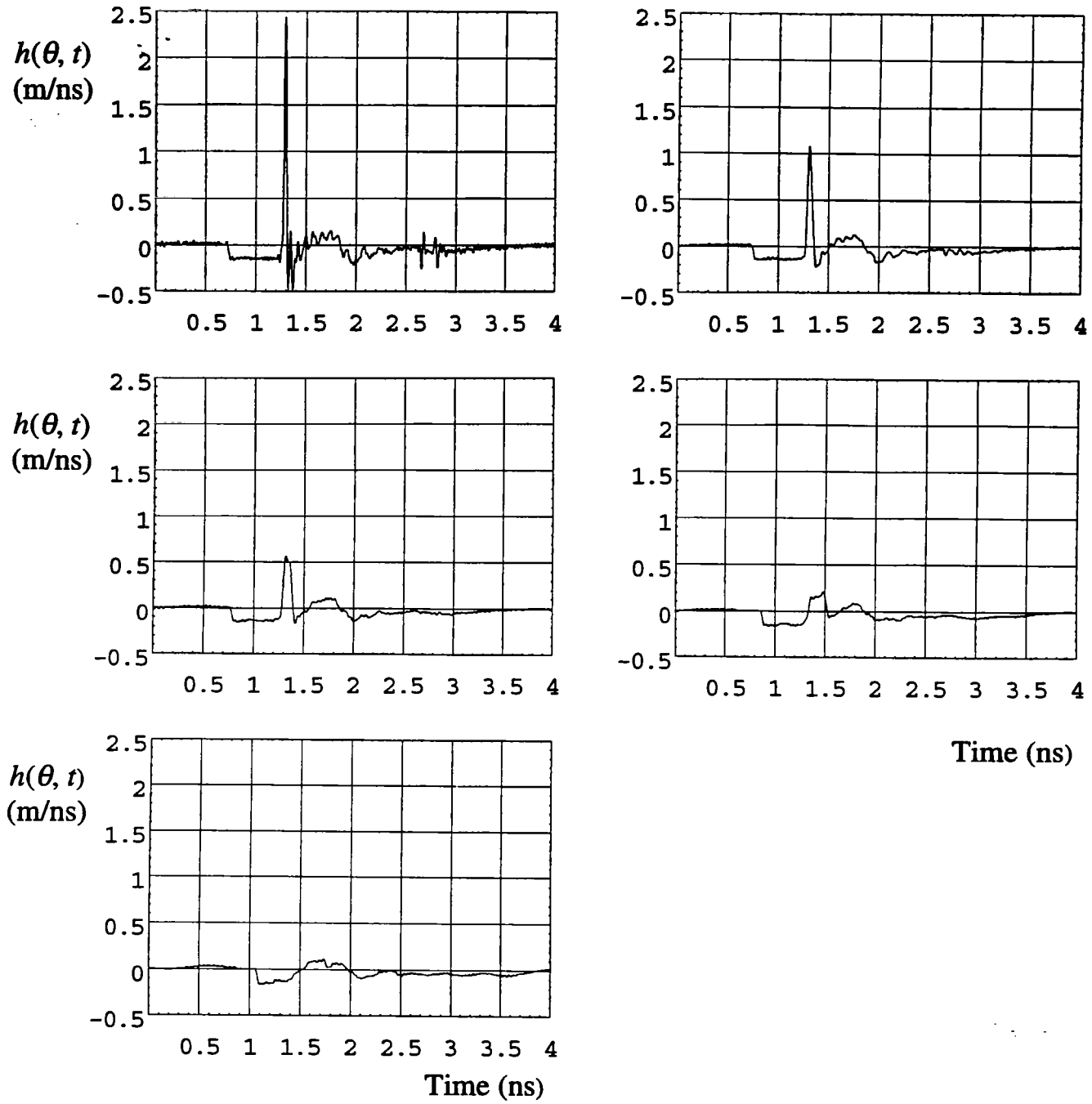

Figure 4.8(a) E-plane $h(\theta, t)$ at 0, 5, 10, 20, and 40 degrees off-boresight.

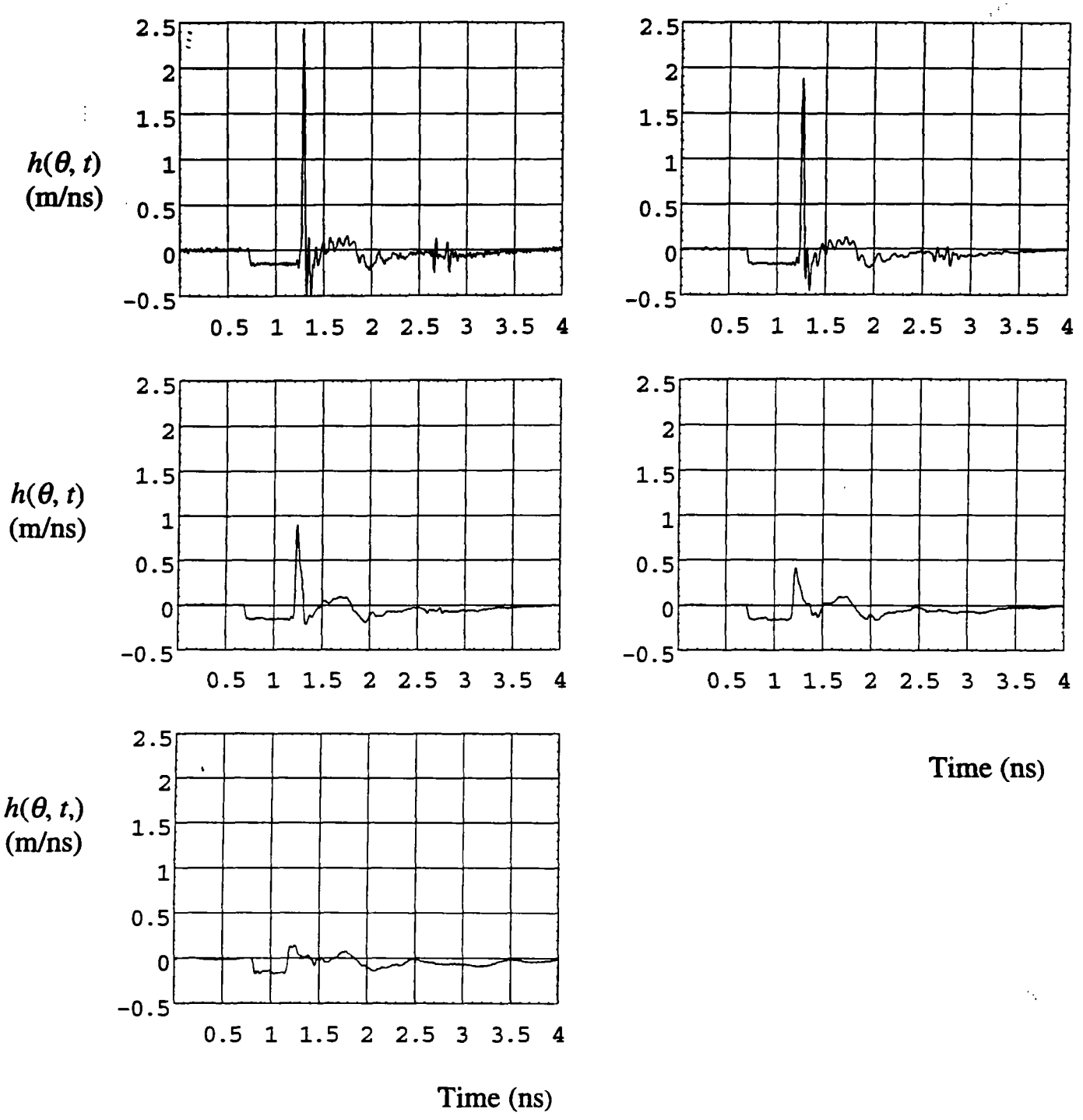

Figure 4.8(b) H-plane $h(\theta, t)$ at 0, 5, 10, 20, and 40 degrees off-boresight.

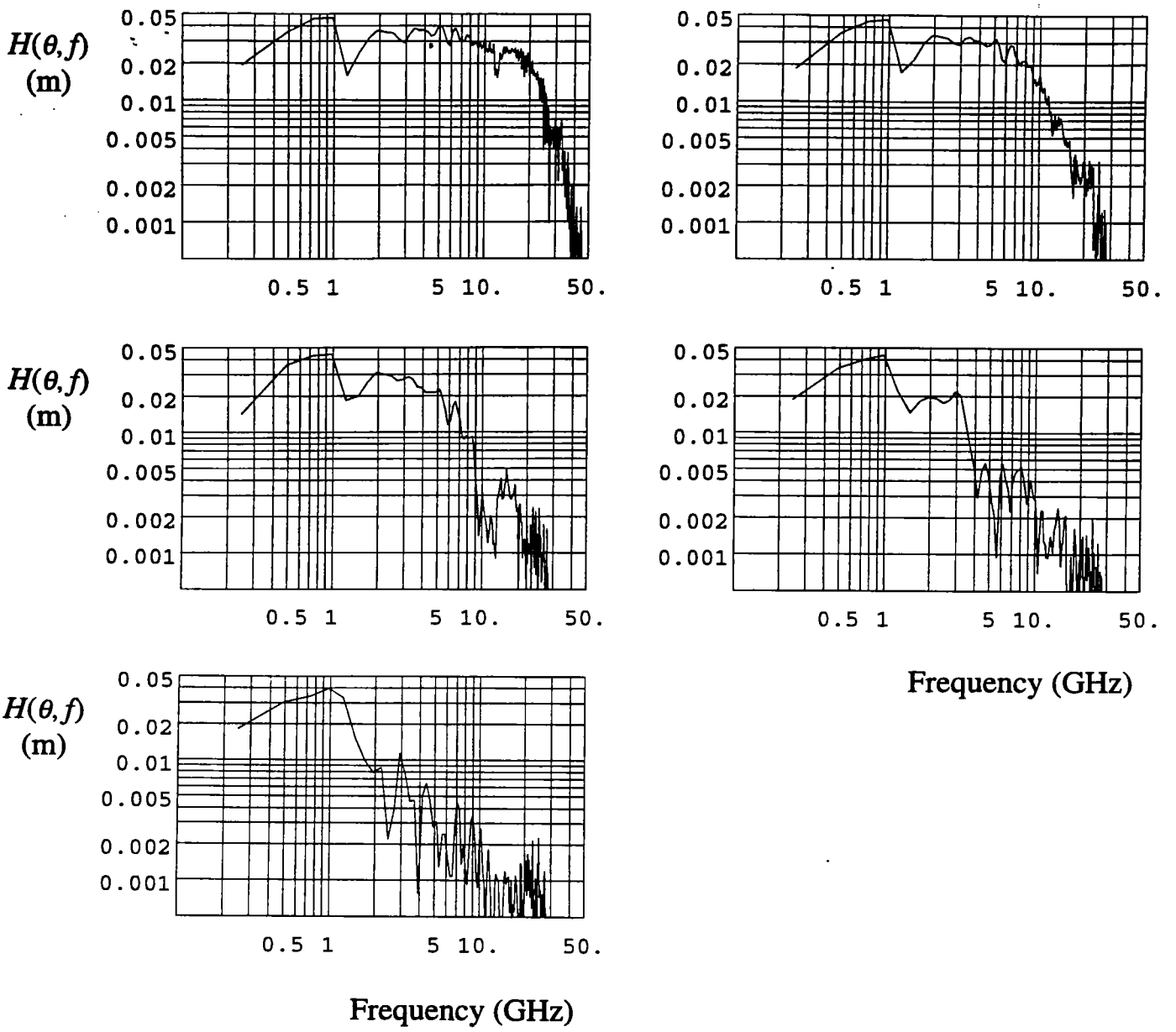

Figure 4.9(a) E-plane $H(\theta, f)$ at 0, 5, 10, 20, and 40 degrees off-boresight.

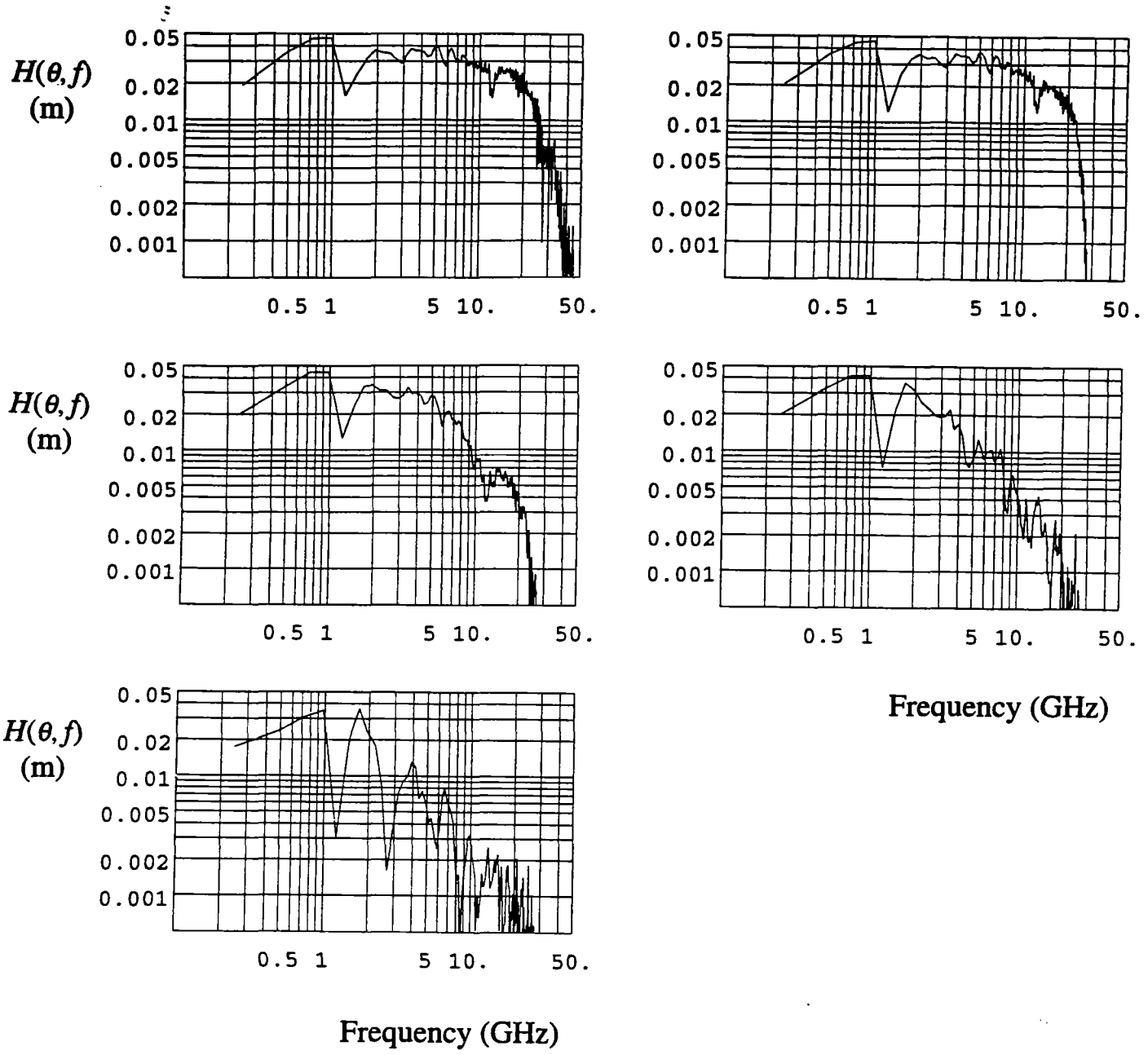

Figure 4.9(b) H-plane $H(\theta, f)$ at 0, 5, 10, 20, and 40 degrees off-boresight.

V. Additional Measurements and Data Interpretation for the Reflector IRA

We consider here some additional calculations and measurements associated with the reflector IRA.

First, we calculate the gain pattern of the reflector IRA. We do so in two ways. First, we plot the peak magnitude of $h(\theta,t)$ in the E- and H-planes, for the five angles shown in Figures 4.8(a) and 4.8(b). The result is shown in Figure 5.1. If the beamwidth is defined as the width where the pattern is down by 0.707 from the peak (half power), then the half-beamwidth is about 3 degrees in the E-plane and 5 degrees in the pseudo H-plane. This beamwidth will occur with an ideal step-function excitation voltage.

Next, we consider a more meaningful definition of gain, as was defined in [5]. This is useful for the more practical case of a finite risetime pulser. Thus, we convolve the response of the antenna with a Gaussian of finite risetime, in this case 50 ps. The precise definition in receive mode is

$$G(\theta) = \frac{1}{\sqrt{f_g}} \frac{\|V_{rec}(t)\|}{\|E_{inc}(\theta,t)\|} = \frac{1}{\sqrt{f_g}} \frac{\|h(\theta,t) \circ E_{inc}(t)\|}{\|E_{inc}(t)\|} \tag{5.1}$$

where we interpret the norm symbol $\| \ \|$ as simply taking the peak of a waveform. Furthermore, it was shown in [5] that this is equivalent to the following definition in transmit mode

$$G(\theta) = \lim_{r \to \infty} \frac{2\pi c \sqrt{f_g} \| r\, E_{rad}(\theta,t) \|}{\| dV_{inc}(t)/dt \|} = \frac{\|h(\theta,t) \circ dV_{inc}(t)/dt \|}{\sqrt{f_g} \| dV_{inc}(t)/dt \|} \tag{5.2}$$

Either way, the gain is simply a convolution of $h(\theta, t)$ with a Gaussian whose integral has a derivative risetime of 50 ps, with appropriate normalization. The results are shown in Figure 5.2. If we define the beamwidth as angle where the pattern is down by a factor of 0.707, the half beamwidths are 5 degrees in the E-plane, and 8 degrees in the pseudo H-plane. Thus, we see that as the driving voltage becomes broader, the antenna beam also becomes more broad. We estimate that for a 100 ps risetime pulser the beamwidth will be approximately twice these values.

Next, we show the Time Domain Reflectometry data for the reflector IRA. The experimental setup is shown in Figure 5.3, and the results are shown in Figure 5.4. This data is simply the raw data, since the normalization procedure changes the waveform only slightly.

Finally, we verify that we were truly in the far field, when we made our measurements at a distance of 6.63 m. To do so, we simply measure the received voltage on boresight, using the two-antenna measurement technique of the previous section, while varying the distance. The measurement was made above the wooden deck at a height of 4.37 m (172 in) above the ground, using the instrumentation setup shown in Figure 3.1. The raw received voltage is shown in

Figure 5.5. To check if the received voltage follows $1/r$, we plot $r \times V_{max}$, where V_{max} is the maximum received voltage. This is shown in Figure 5.6. From the diagram, we see that distances over 3 m have a constant $r \times V_{max}$, so we infer that this is the beginning of the far field.

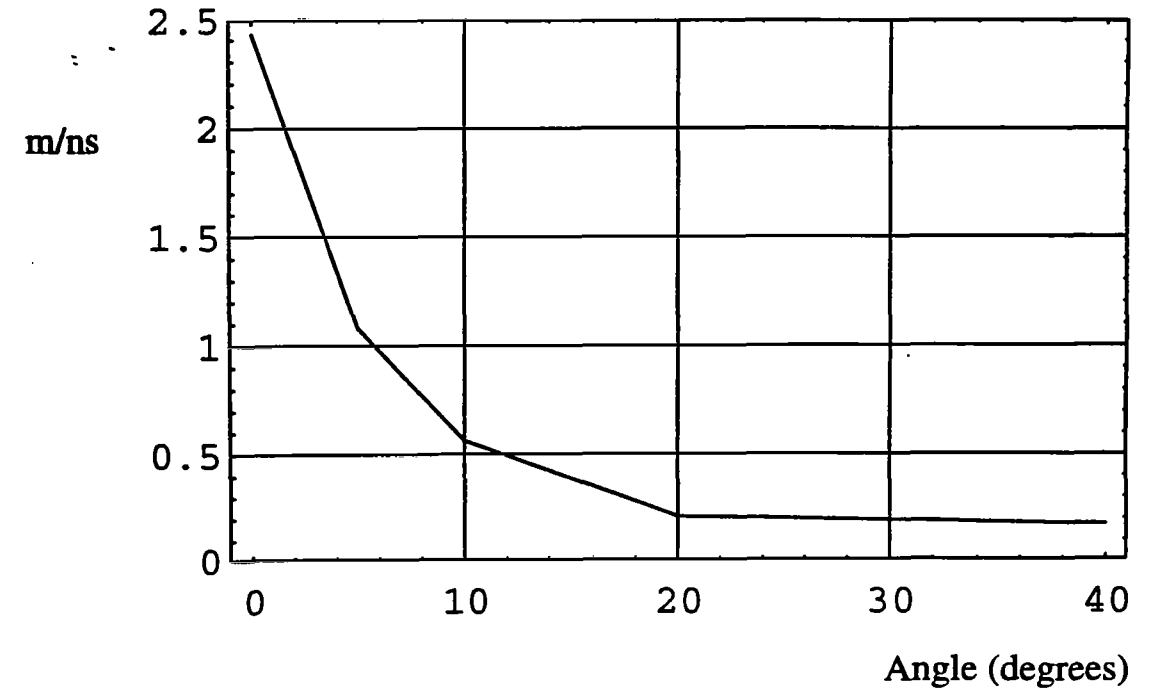

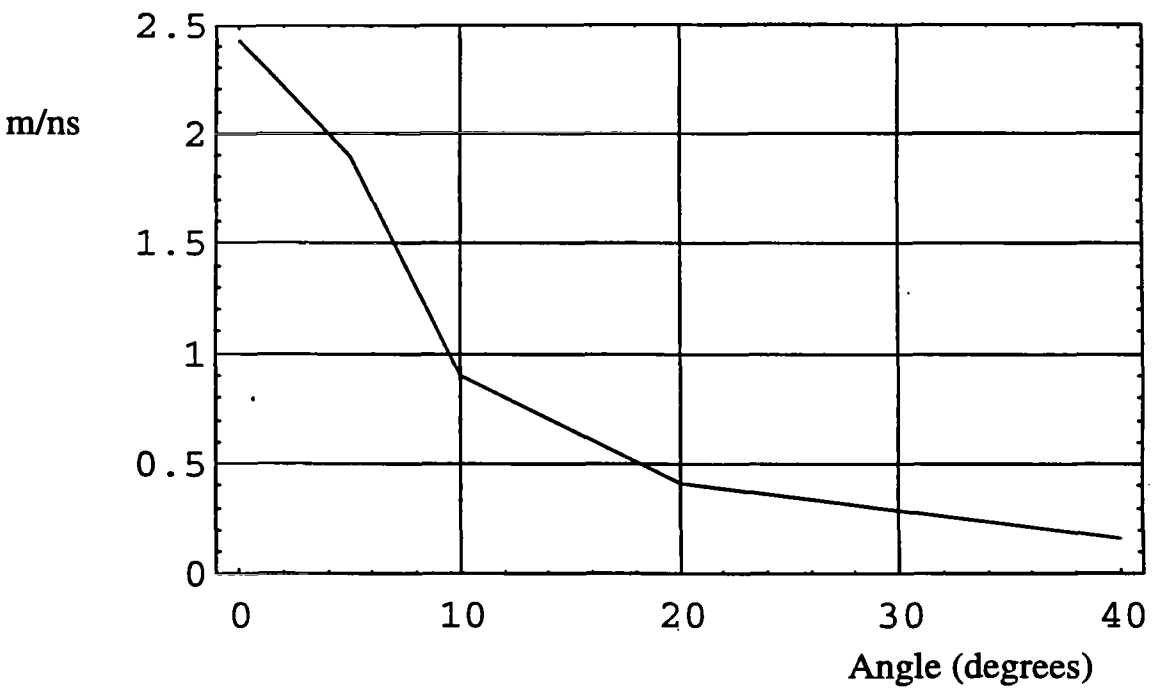

Figure 5.1. Gain of the 23 cm (9-in) reflector IRA plotted as a function of angle off-boresight in the E-plane (top) and in the pseudo H-plane (bottom). Here gain is used in the peak $h(t)$ sense.

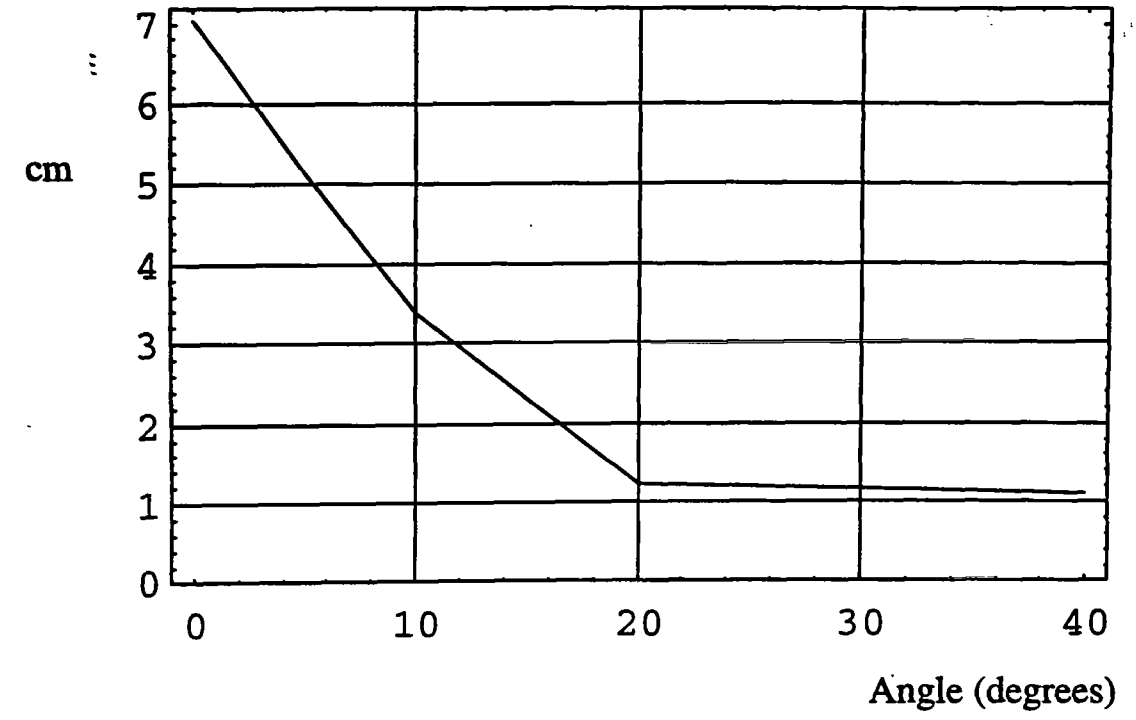

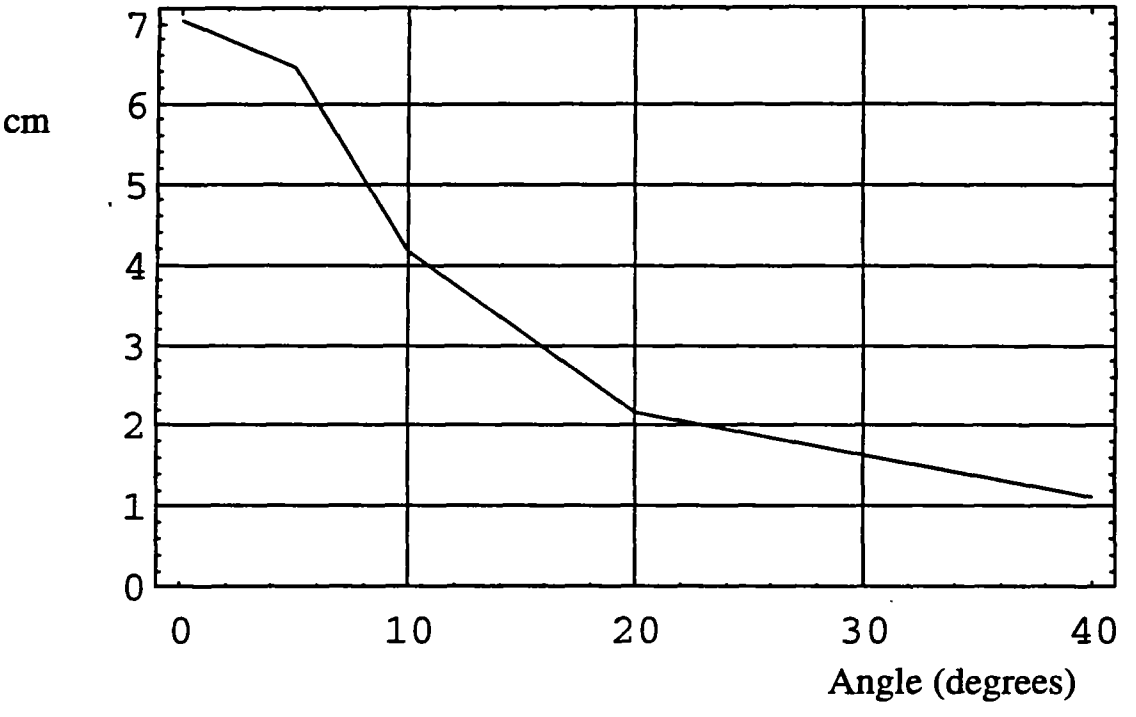

Figure 5.2. Gain of the 23 cm (9 in) reflector IRA plotted as a function of angle off-boresight in the E-plane (top and in the pseudo H-plane (bottom). Here gain is as defined in Equation 5.1.

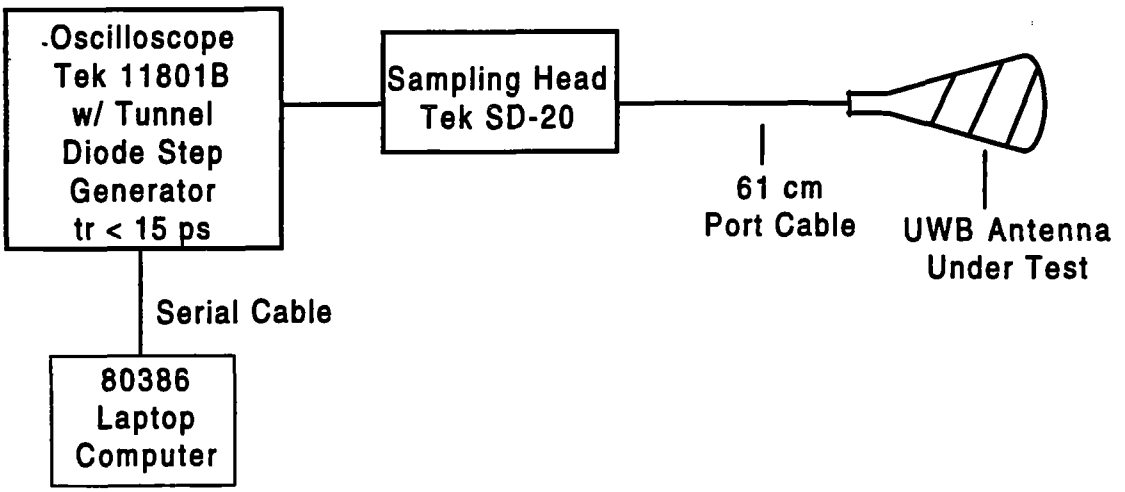

Figure 5.3. Experimental configuration for TDR measurements.

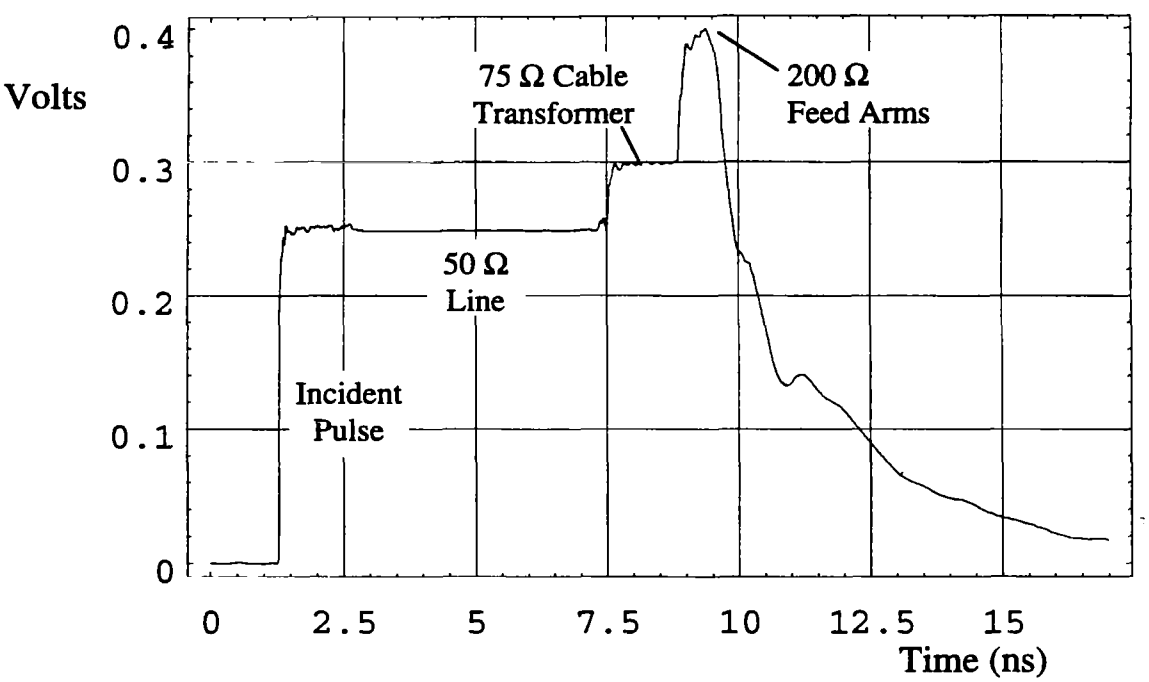

Figure 5.4. TDR of the reflector IRA.

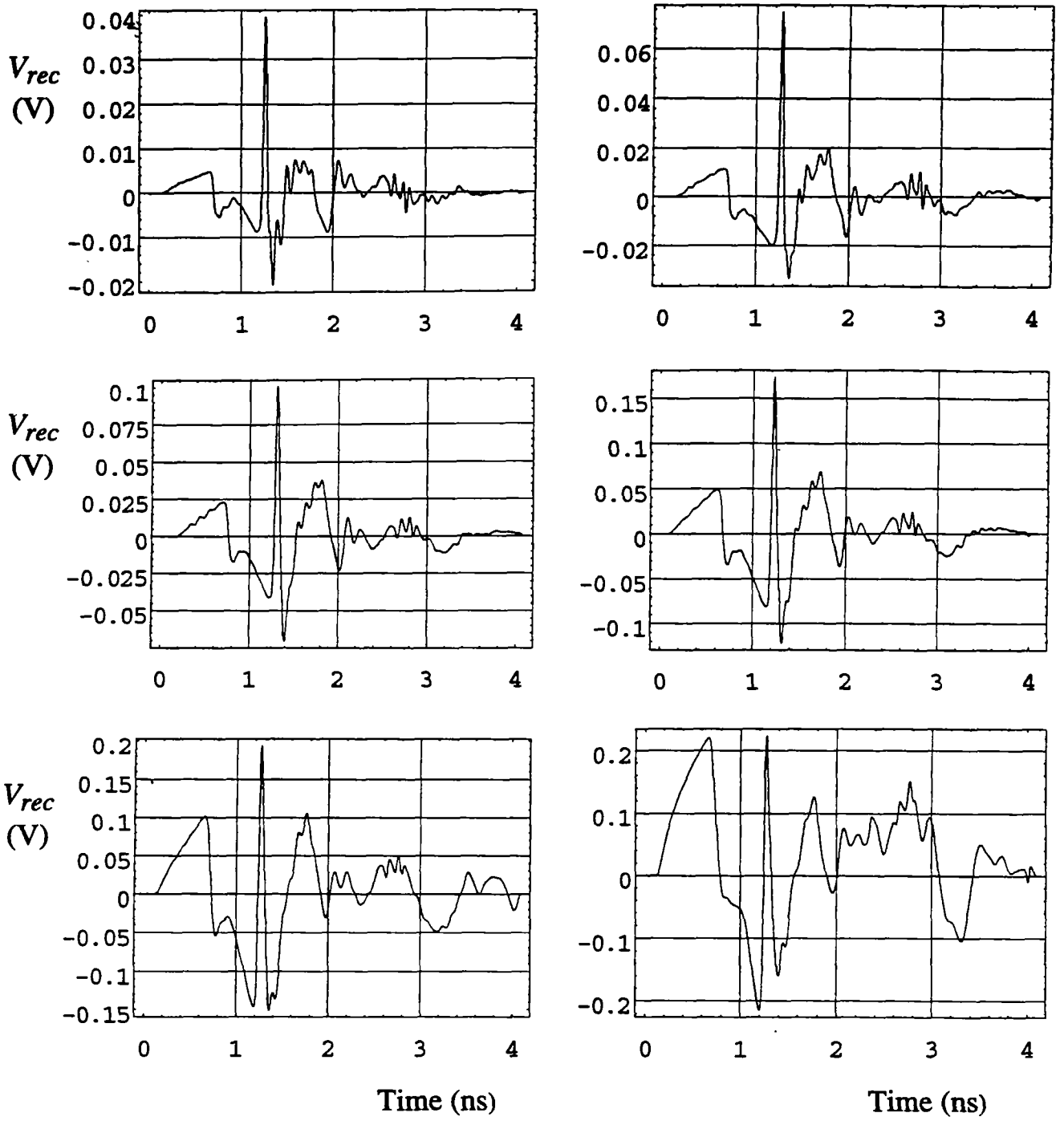

Figure 5.5. Received voltage in the two-antenna measurement, as a function of antenna separation. The distances were 5.66, 2.87, 1.45, 0.71, 0.36, and 0.18 meters.

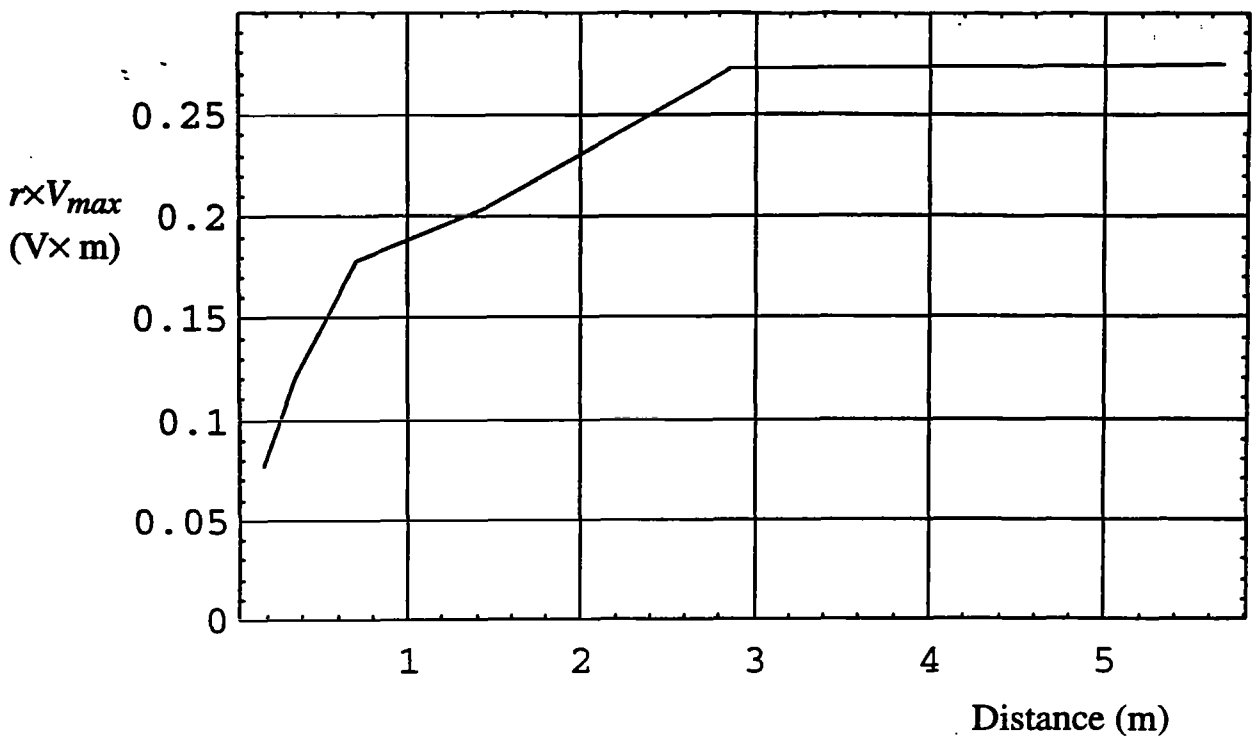

Figure 5.6. A check on the $1/r$ dependence of the measurement. Based on this, measurements over 3 m are in the far field.

VI. Lens IRA Theory

Two identical lens IRAs were built, as described in [1]. The only modifications from what was originally described in [1] was that the TEM horn was terminated in two 192 Ω resistors, which provided a total impedance of 96 Ω at low frequencies. The region around the apex was filled with paraffin wax, which has approximately the same dielectric constant as polyethylene. This reduced significantly the precursor that was otherwise seen.

Let us build up the equations for the lens IRA, analogous to what was done in Section II of this paper. We consider here a configuration where the upper and lower plates each have the optimal angular width of 90 degrees. First, the radiated field on boresight is [1]

$$\begin{aligned} E_{rad}(t) &= -\frac{0.85\, a\, \tau}{2\pi r c f_g} \frac{d V_{inc}^{(feed)}(t)}{dt} \\ \tau &= \frac{2}{1+\sqrt{\varepsilon_r}} \end{aligned} \tag{6.1}$$

where a is the aperture radius, f_g is the normalized impedance of the TEM horn as embedded in the dielectric (optimal $f_g = 1/(2\sqrt{\varepsilon_r})$), $V_{inc}^{(feed)}(t)$ is the voltage across the uniform TEM feed, and τ is the transmission coefficient from air to dielectric material. Note that we are constrained to use the optimal f_g in the above equation, because the factor of 0.85 is specific to that case. We must also account for impedance discontinuities in the feed cables. That is, the feed impedance transitions from 50 Ω to 75 Ω, and from 75 Ω to 124 Ω. We account for this as an extra transmission coefficient τ_{t1}, so we now have

$$E_{rad}(t) = -\frac{0.85\, a\, \tau\, \tau_{t1}}{2\pi r c f_g} \frac{d V_{inc}^{(cable)}(t)}{dt} \tag{6.2}$$

and we will calculate the value of τ_{t1} later. The above equation is alternatively expressed as

$$\begin{aligned} E_{rad}(t) &= -\frac{\tau_{t1}}{2\pi r c f_g} h(t) \circ \frac{d V_{inc}^{(cable)}(t)}{dt} \\ h(t) &= 0.85\, \tau\, a\, \delta(t) \end{aligned} \tag{6.3}$$

where $\delta(t)$ is the Dirac delta function and " $\circ$ " indicates a convolution. This is the final result we use to describe the antenna's behavior on boresight in transmission.

In reception, the received voltage across the TEM feed is

$$V_{rec}^{(feed)}(t) = 0.85\, \tau\, a\, E_{inc}(t) \tag{6.4}$$

This is modified by the transmission coefficient from the feed to the cable, to obtain

$$V_{rec}^{(cable)}(t) = -0.85\,\tau\,\tau_{t2}\,a\,E_{inc}(t) \tag{6.5}$$

where τ_{t2} is the ratio of the voltage excited on the feed arms to the voltage in the 50 Ω cable. Using the same $h(t)$ which was used previously in (2.4), we have

$$\begin{aligned} V_{rec}^{(cable)}(t) &= \tau_{t2}\,h(t) \circ E_{inc}(t) \\ h(t) &= 0.85\,a\,\tau\,\delta(t) \end{aligned} \tag{6.7}$$

Finally, we expand the above $h(t)$ to include the postpulse, which is approximated as

$$h(t) = 0.85\,a\,\tau\left[\delta(t) - \frac{c}{2\ell\sqrt{\varepsilon_r}}\left[u(t) - u(t - 2\ell\sqrt{\varepsilon_r}/c)\right]\right] \tag{6.8}$$

where ℓ is the distance from the feed point (focus) to the front edge of the lens. This is the function we will need to extract from the measured data.

As with the reflector, using the two-antenna method [2], we will measure on boresight

$$V_{rec}^{(cable)}(t) = \frac{\tau_{t1}\,\tau_{t2}}{2\pi r c f_{g2}}\,h(t) \circ h(t) \circ \frac{dV_{inc}^{(cable)}}{dt} \tag{6.9}$$

Thus, in the experiment we can use the measured cable voltages to extract $h(t)$, the boresight response. When we scan in the E- or H-plane, we have to modify one of the $h(t)$s to indicate a response off-boresight. Thus, we measure

$$V_{rec}^{(cable)}(t) = \frac{\tau_{t1}\,\tau_{t2}}{2\pi r c f_{g2}}\,h(t) \circ h^{(e)}(t,\theta) \circ \frac{dV_{inc}^{(cable)}}{dt} \tag{6.10}$$

in the E-plane, where $h^{(e)}(\theta, t)$ is the antenna characteristic as a function of angle θ off boresight in the E-plane. An analogous expression using $h^{(h)}(\theta,t)$ is true in the H-plane.

The transmission coefficients for the impedance discontinuities, τ_{t1} and τ_{t2}, are now calculated with equation (2.12) in a manner exactly analogous to that used for the reflector antenna. Thus, the transmission coefficients are

$$\begin{aligned} \tau_{t1} &= \frac{2\times 75}{50+75}\times\frac{2\times 124}{75+124} = 1.495 \\ \tau_{t2} &= \frac{2\times 75}{124+75}\times\frac{2\times 50}{75+50} = 0.603 \\ \tau_{t1}\times\tau_{t2} &= 0.902 \end{aligned} \tag{6.11}$$

Thus, there is a two-way loss in voltage of 0.902 due to impedance discontinuities in the feed cables.

VII. Experimental Setup for the Lens IRA

Data for the lens IRAs was acquired as described for the reflector IRAs using the instrumentation setup shown in Figure 3.1, with the physical setup as shown in Figure 7.1. This configuration allows a purely horizontal path. The lens antennas were separated by 5.0 meters (197 in) on a wooden deck. The horizontal path between the two antennas was 1.55 meters (61 in) above the wooden deck and 4.3 m (172 in) above the ground level. Reflections from the wood deck were seen to be insignificant, while all other reflections (including those from the ground) were outside the 5 ns observation window. The use of a horizontal path allowed pure E- and H-plane scans to be accomplished when the azimuth/elevation mount was rotated about the horizontal and vertical axes. The H-plane data was taken with ± 2.5 degree angular accuracy, using a protractor scale. The E-plane data was taken with ± 0.5 degree angular accuracy using a gravity inclinometer.

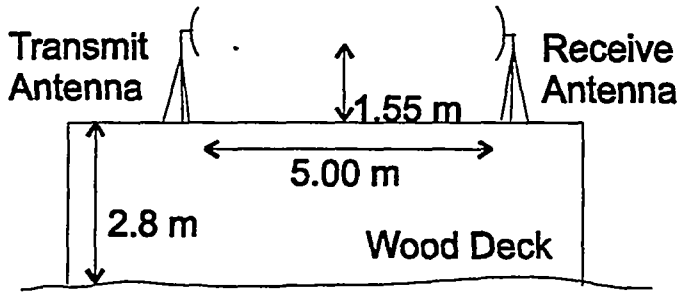

Figure 7.1. The physical layout of the two antennas for the lens IRA measurements.

VIII. Results for the Lens IRA

The process of taking the data for the lens IRA was exactly the same as that for the reflector IRA, as described in Section IV. The only exception is that the lens IRA could be scanned in a true H-plane. The details of the signal processing are also largely the same as those in Section IV, except as noted below.

The step function normalization waveform is shown in Figure 8.1 (top). The derivative of the resulting waveform, after filtering with the modified Butterworth with $N = 10$ and $f_o = 30$ GHz is shown in Figure 8.1 (middle). The modified Butterworth filter was shown previously in equation (4.1). Finally, a frequency spectrum of the waveform is shown on the bottom of Figure 8.1. This spectrum is for the complete measurement system response, including source, sampler, and cabling.

The raw received voltages for the E-plane are shown in Figure 8.2.(a), and a closeup of the peaks is shown in Figure 8.2(b). This is repeated for the H-plane data in Figures 8.2(c) and 8.2(d). These data sets have all been filtered in the frequency domain by the modified Butterworth filter, with $N = 10$ and f_o=30 GHz. Comparison of Figure 8.2 to with Figure 4.2 shows a much higher peak received signal for the lens antenna.

The frequency spectra for the E-plane and H-plane patterns are shown in Figures 8.3(a) and 8.3(b). As with the reflectors, the high frequencies are lost at the wider angles.

The next step is to normalize the waveforms to the derivative of the system response, as provided earlier in Figure 8.1(middle). The normalized E-plane response is shown in Figures 8.4(a) and 8.4(b), and the normalized H-plane response is shown in Figures 8.4(c) and 8.4(d). These waveforms are what would be seen with a perfect step source and measurement system, with 5.0 meter (197 in) antenna separation. These waveforms are unitless, but if a one-volt perfect step were used to excite the transmit antenna, these waveforms would show the output of the receive antenna in volts.

From these waveforms we can measure the FWHM for the on- and off-boresight cases. The results are shown in Table 8.1. Note that the waveforms are assumed to begin at a level of –0.005. This corrects for a pedestal preceding the impulse that starts below zero. Finally, we show the corrected spectra of the receive signal, as shown in Figures 8.5(a) and 8.5(b). Once again, we see that the high frequencies fall off sharply at wide angles.

Table 8.1. Pulse Widths of the Received Voltages as a Function of Angle, After Normalization.

	Angle (deg)	t_{FWHM} (ps)
E-Plane	0.0	29
	2.5	31
	5.0	62
	7.5	94
	10.0	121
H-Plane	0.0	29
	5.0	68
	10.0	101

Next, we extract the $h(t)$ for the antenna, which is the step response in transmission, or the impulse response in reception, as shown in Equation (6.9). To do so, we obtained $H(f)^2$ in the frequency domain by multiplying the normalized received voltage by $2\pi rcf_g/\tau_{t1}\tau_{t2}$, where f_g = 124/376.727, and all the other parameters are defined near Equation (6.9). After unwrapping the phase and taking the square root, the resulting $H(f)$, with phase unwrapped, is shown in Figure 8.6. After converting to the time domain, and restoring the time delay, the boresight impulse response, $h(t)$ is shown in Figure 8.7.

Let us consider now some of the properties of the extracted $h(t)$. We expect for this waveform a sharp impulse, followed by a long postpulse of low amplitude. As with the reflector, it is striking how closely the data resemble what we expect. Our measured $h(t)$ has a FWHM of 21 ps. Note that the FWHM was measured from a baseline of 0.0 m/ns. Furthermore, the area under the impulse is 7.84 cm, also as measured from a baseline of 0.0 m/ns. Simple theory predicts this to be $0.85\,\tau\,a$ = 7.82 cm. Thus, our measurement is 101 % of the impulse area predicted by our theory.

With $h(t)$ derived, we can now extract the antenna pattern data. To do so, we multiply the normalized received voltages of Figure 8.4 by $2\pi rcf_g/\tau_{t1}\tau_{t2}$, and divide in the frequency domain by the Fourier transform of $h(t)$, or $H(\omega)$. At this stage we applied an additional modified Butterworth filter with parameters N = 10 and f_o = 25 GHz. We also applied a limiter to $H(f)$, to avoid dividing by small numbers, as shown earlier in equation (4.2). In this case, we limited $H(f)$ to be no smaller than Max ($|H(f)|$) x 0.01. The frequency response is then converted to the time domain, giving $h(\theta,t)$ as defined by equation (6.10), and the results are shown in Figure 8.8 in the time domain and Figure 8.9 in the frequency domain.

A table of the FWHM of the recovered $h(t)$s is shown in Table 8.2. As expected, the FWHM increases with increasing angle off-boresight.

Table 8.2. Pulse Widths of the $h(\theta,t)$ as a Function of Angle.

	Angle (deg)	t_{FWHM} (ps)
E-Plane	0.0	21
	2.5	28
	5.0	46
	10.0	102
	20.0	216
H-Plane	0.0	21
	5.0	55
	10.0	86
	20.0	204

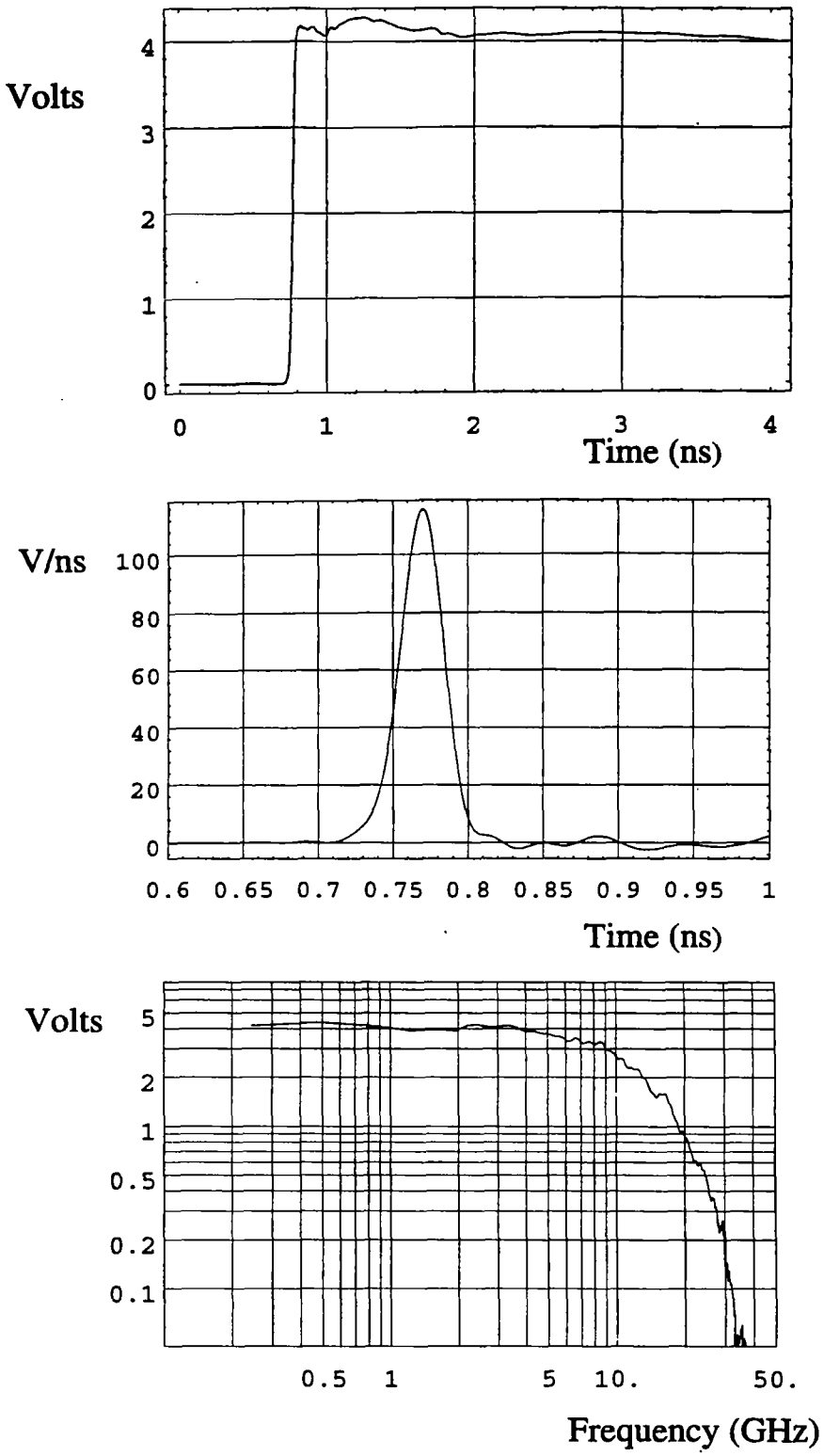

Figure 8.1. The system excitation response (incident voltage and cabling) (top), its derivative after filtering (middle) and its unfiltered frequency spectrum (bottom).

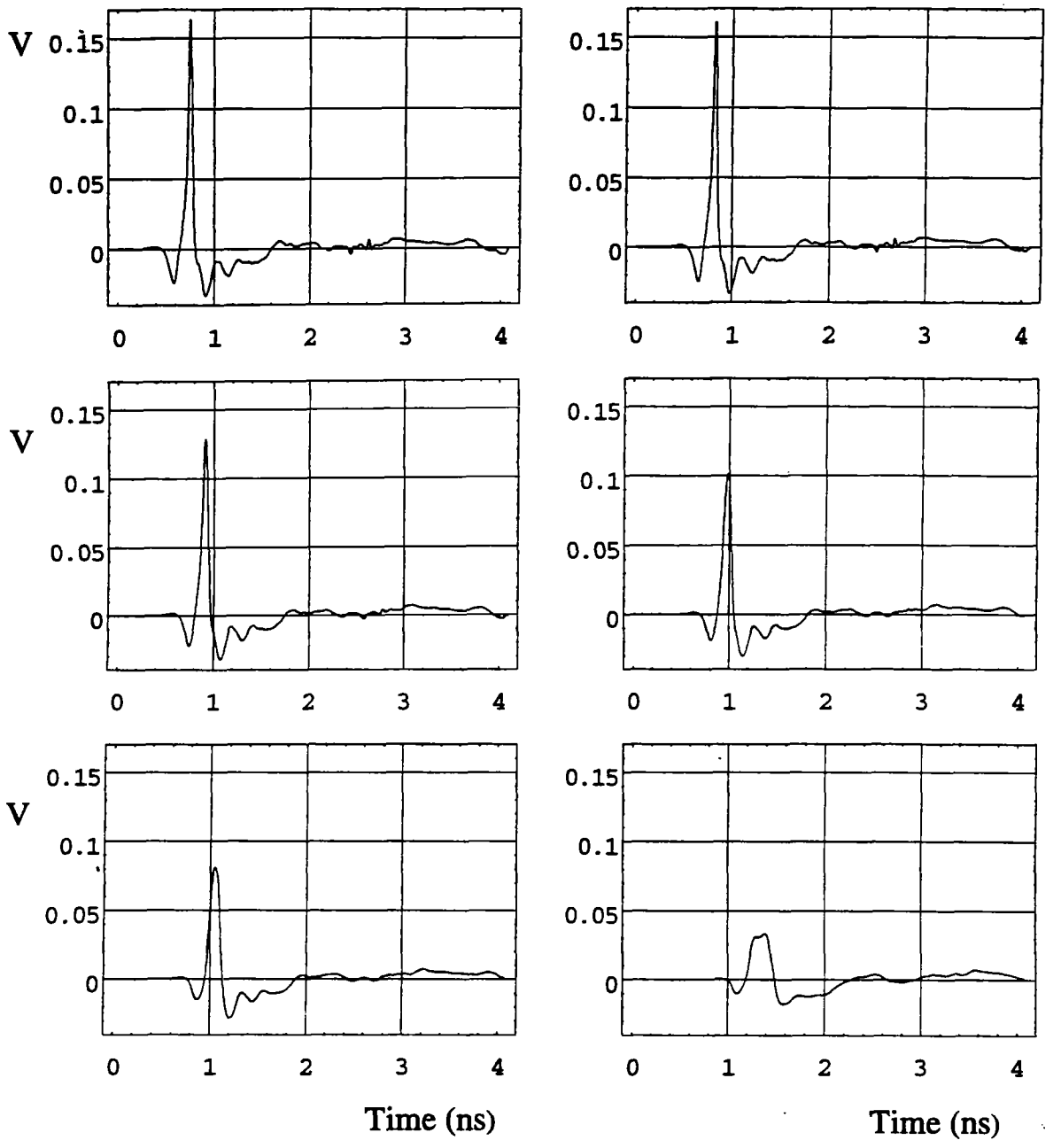

Figure 8.2(a). E-plane received voltage, after filtering. Waveforms are at 0, 2.5, 5, 7.5, 10, and 20 degrees off boresight

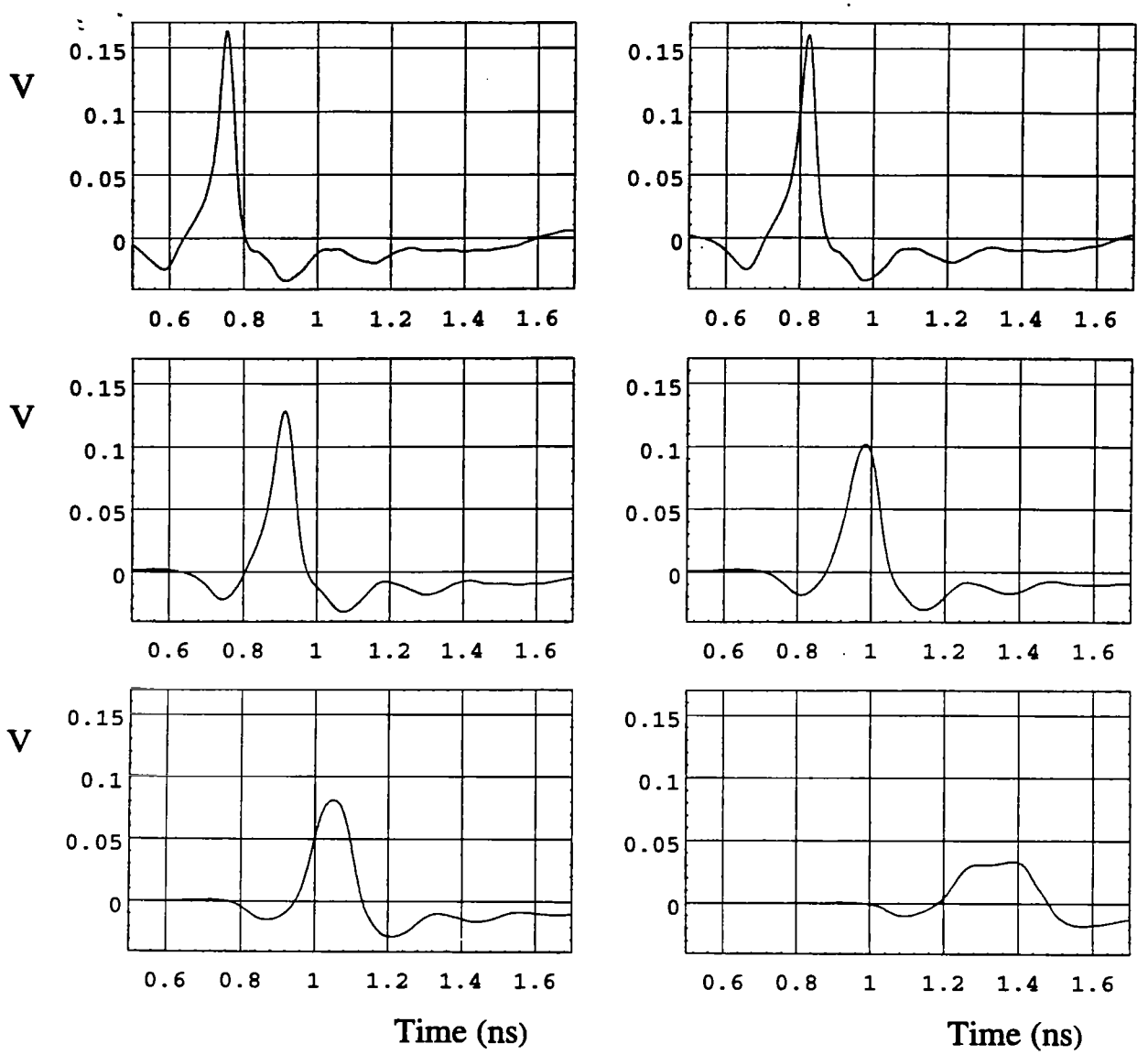

Figure 8.2(b). Closeup of the peaks in Figure 8.2(a).

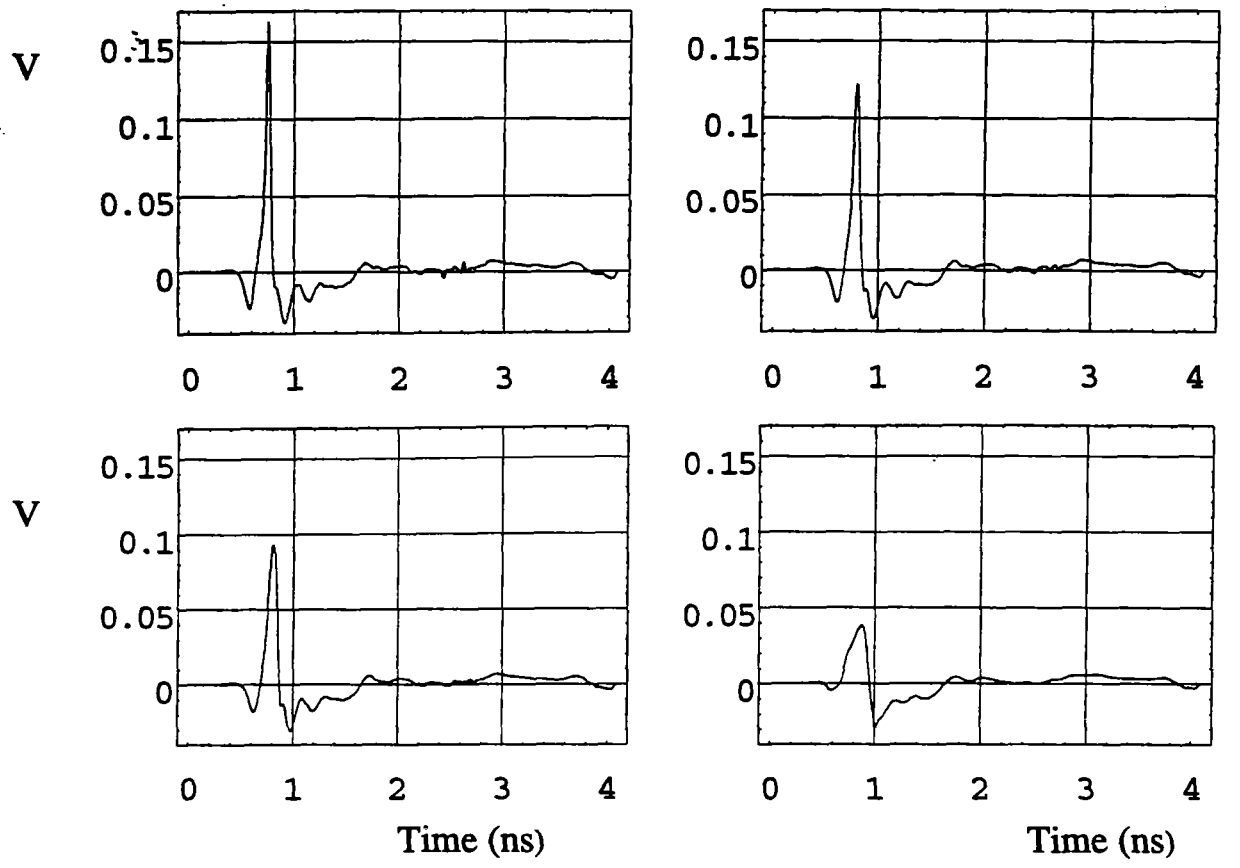

Figure 8.2(c). H-plane received voltage, after filtering. Waveforms are at 0, 5, 10, and 20 degrees off boresight

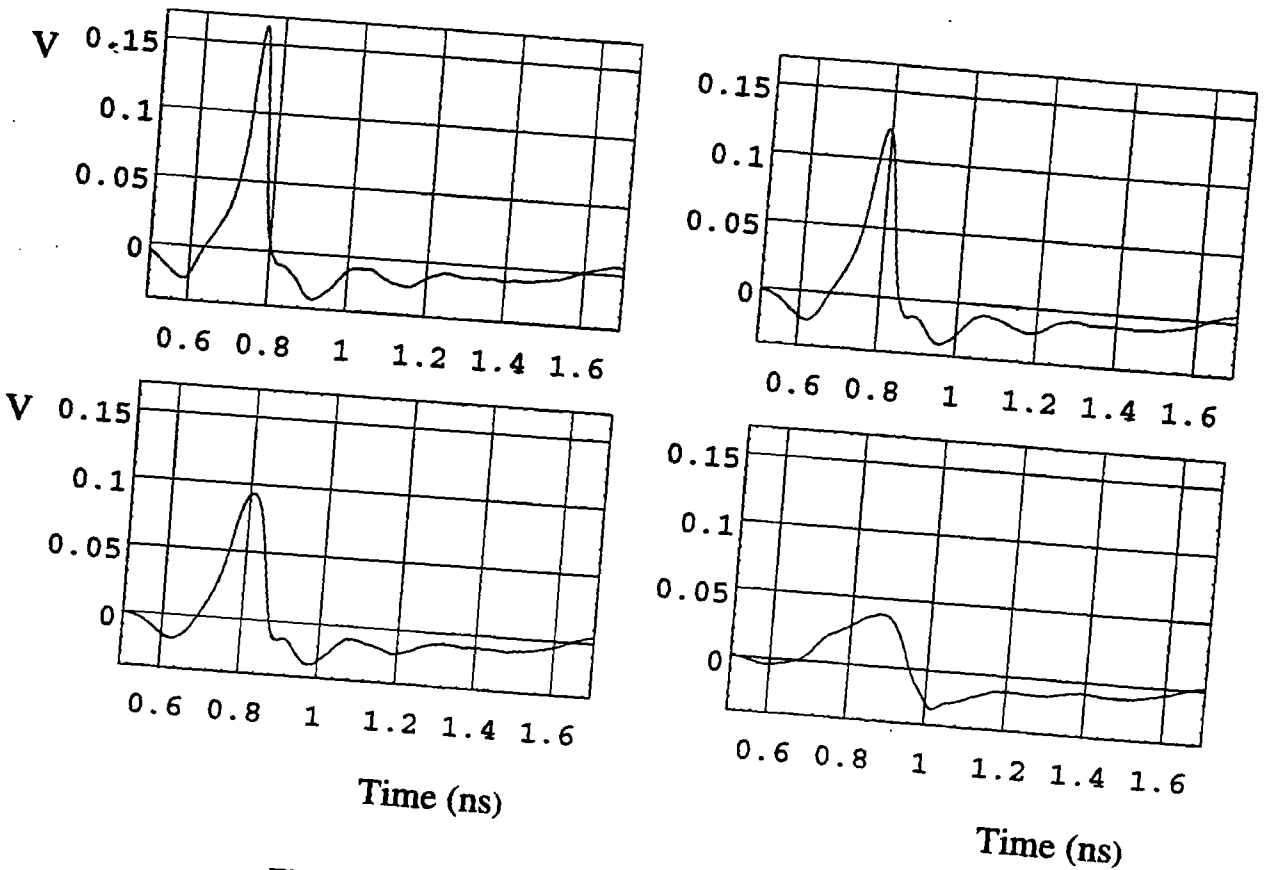

Figure 8.2(d). Closeup of the peaks in Figure 8.2(c).

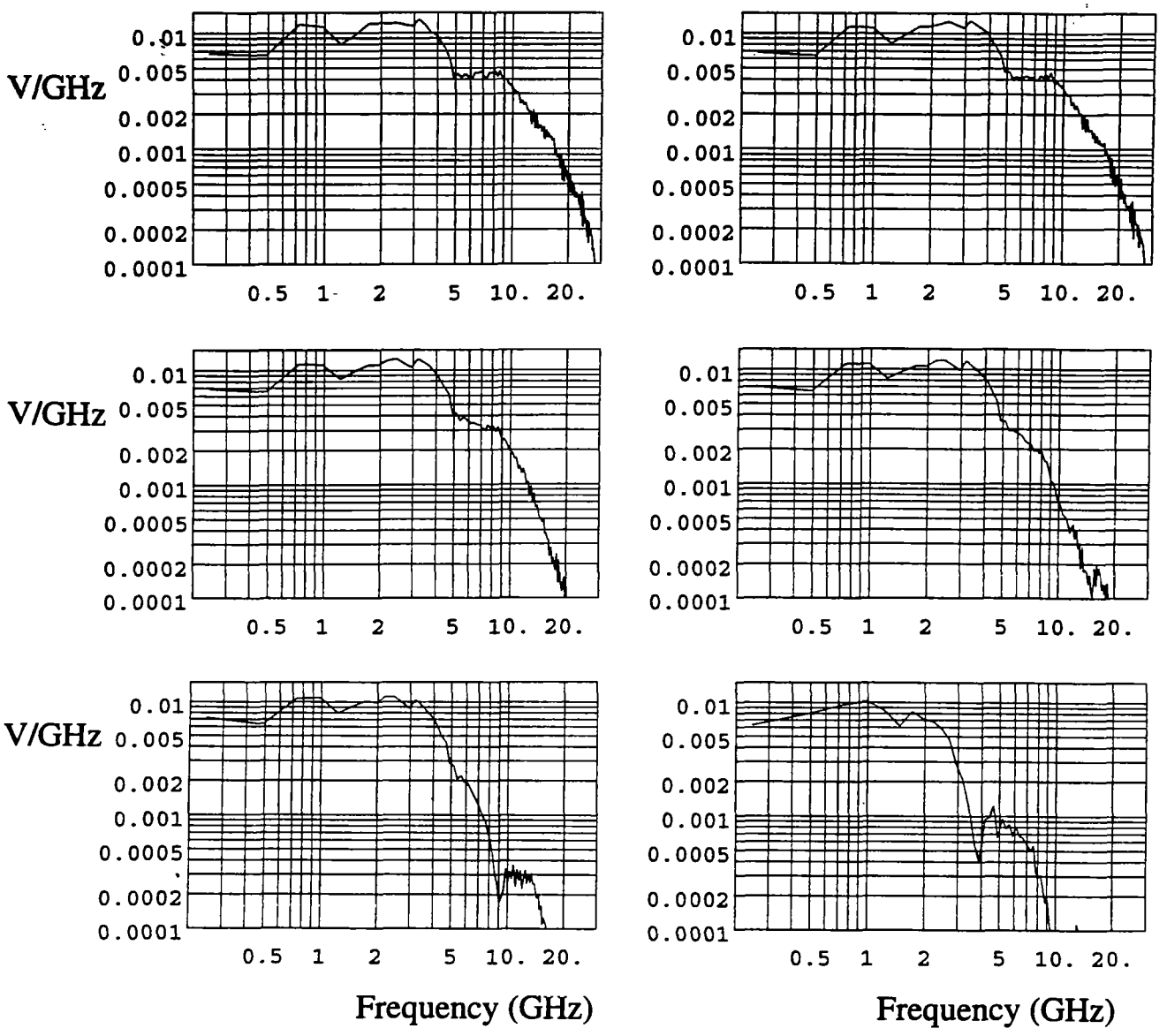

Figure 8.3(a). E-Plane scan, filtered but unnormalized, in the frequency domain. Waveforms are at 0, 2.5, 5, 7.5, 10, and 20 degrees off boresight

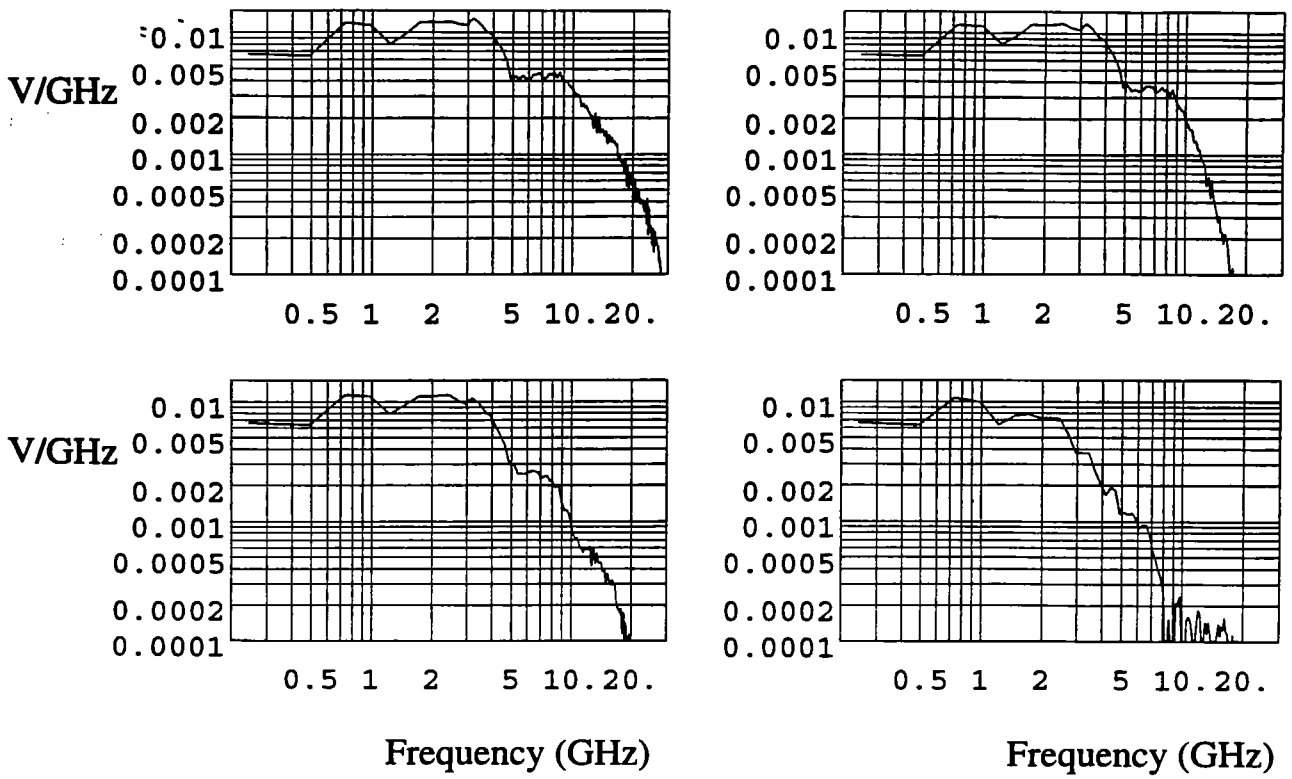

Figure 8.3(b). H-Plane scan, filtered but unnormalized, in the frequency domain. Waveforms are at 0, 5, 10, and 20 degrees off boresight

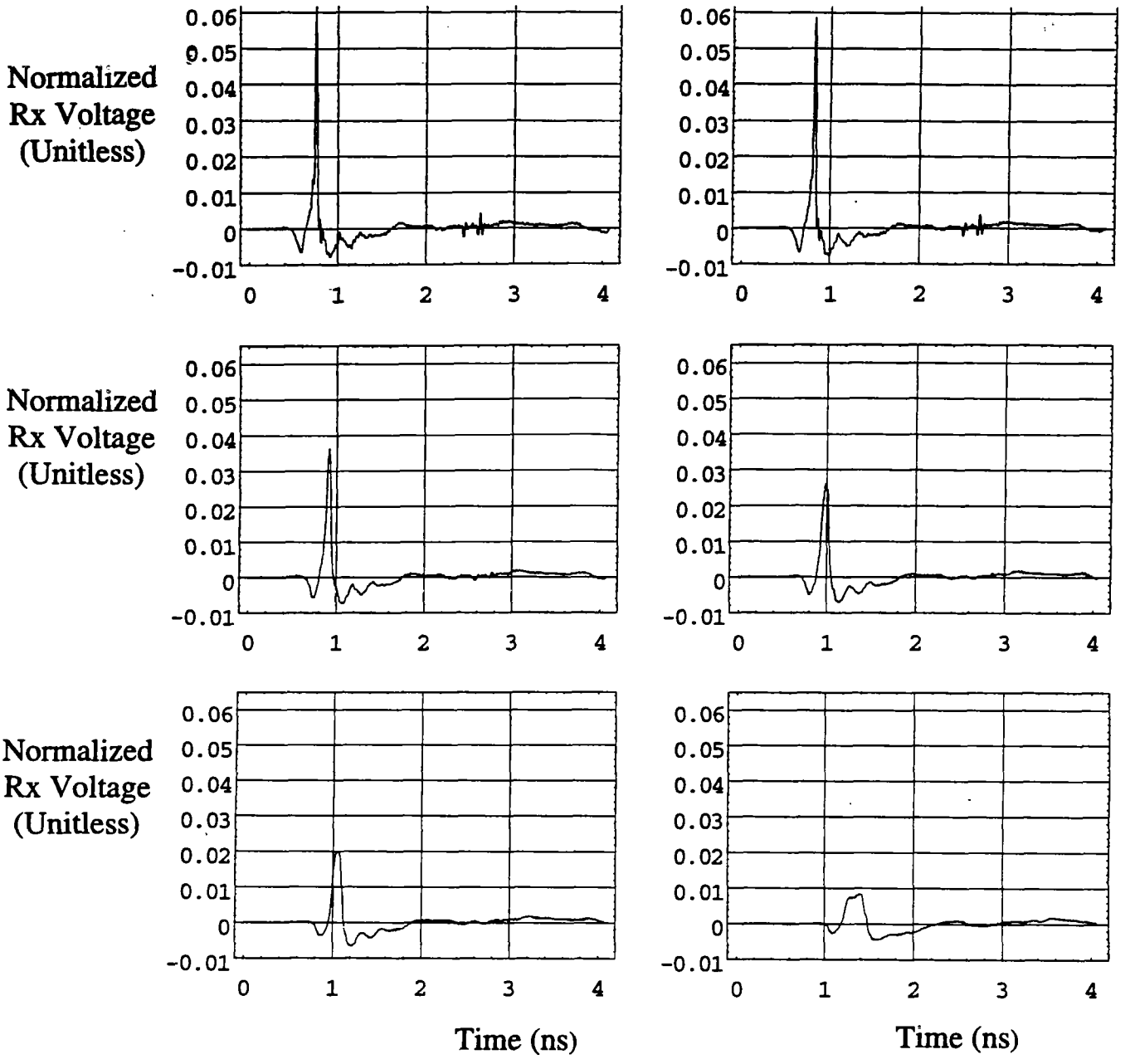

Figure 8.4 (a). E-plane received voltage, after filtering and normalization. Waveforms are at 0, 2.5, 5, 7.5, 10, and 20 degrees off boresight.

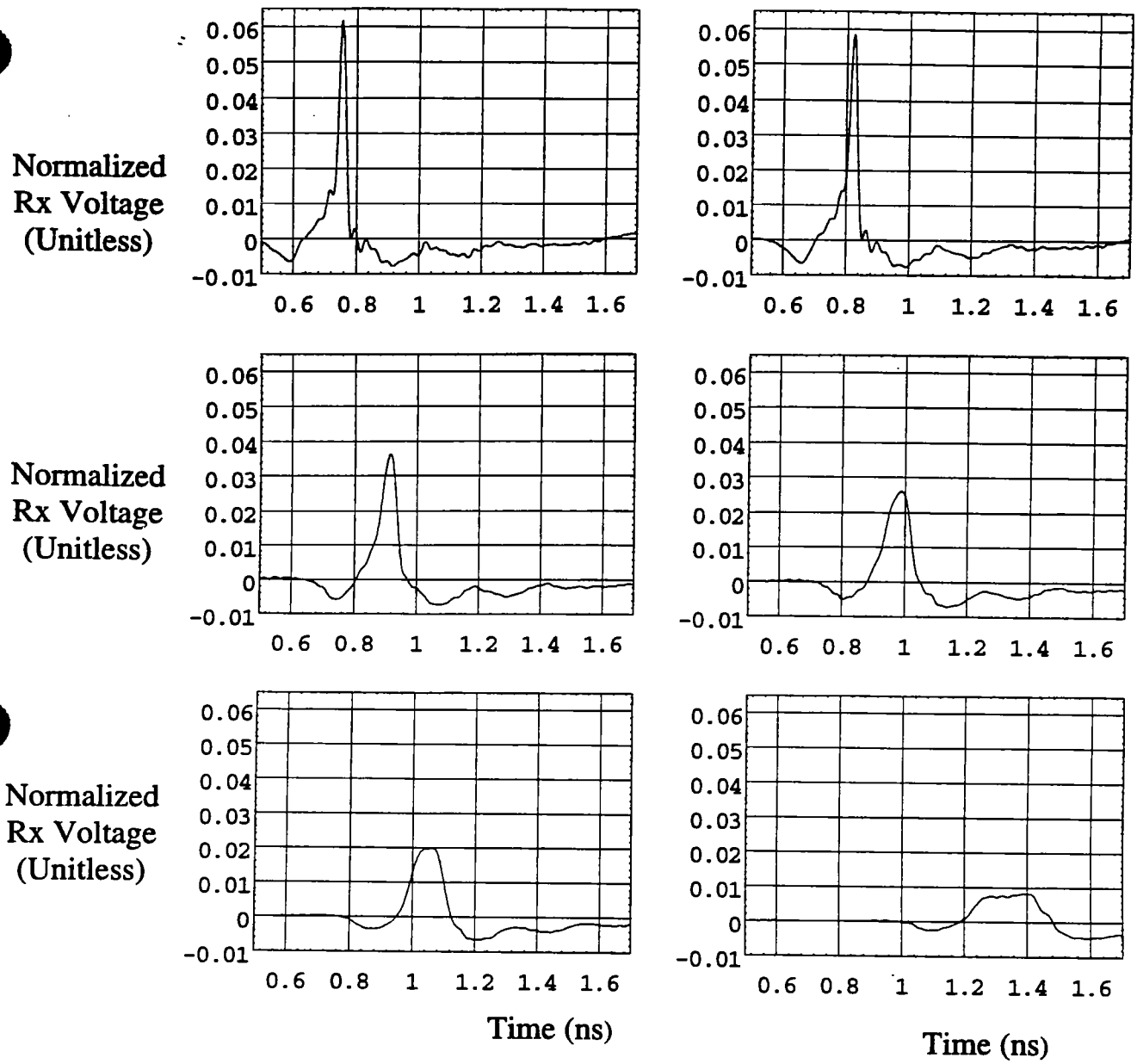

Figure 8.4 (b). Closeup of the peaks in Figure 8.4 (a).

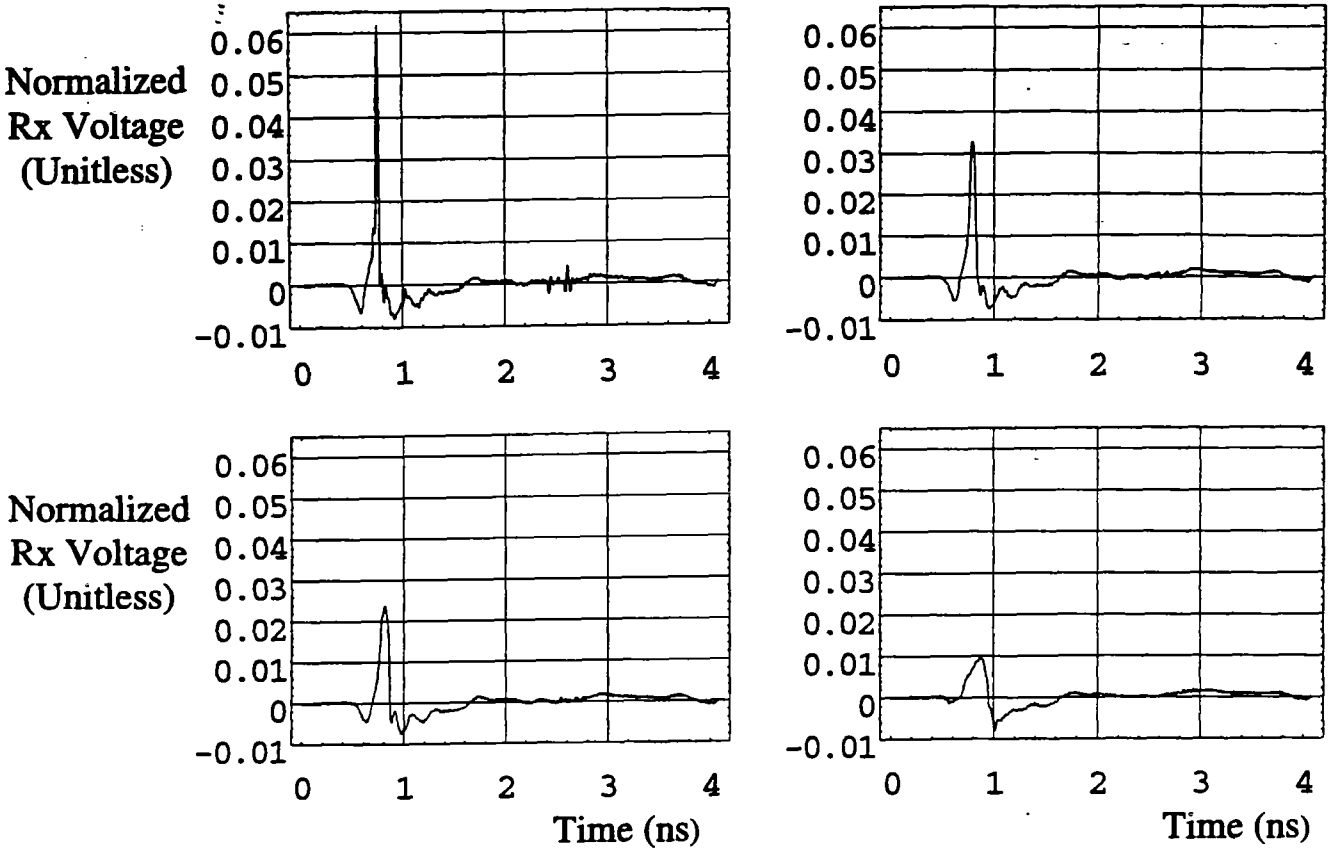

Figure 8.4 (c). H-plane received voltage, after filtering and normalization. Waveforms are at 0, 5, 10, and 20 degrees off boresight.

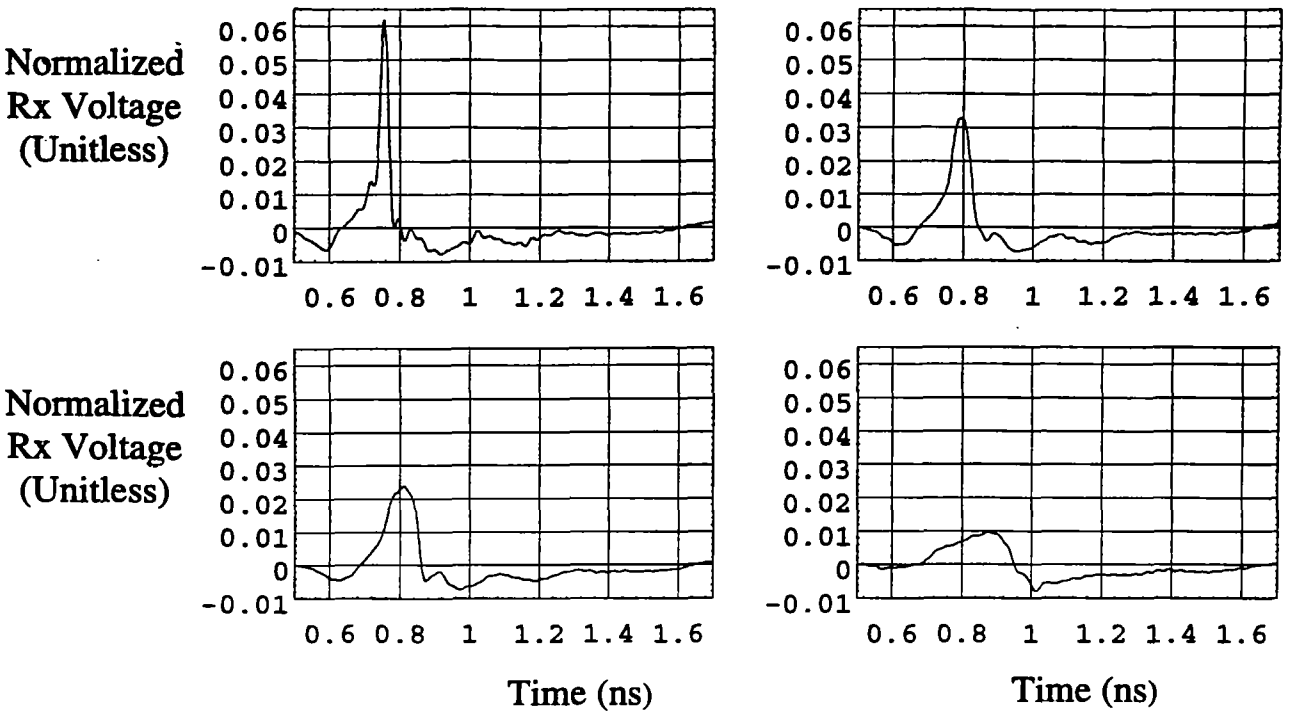

Figure 8.4 (d). Closeup of the peaks in Figure 8.4 (c).

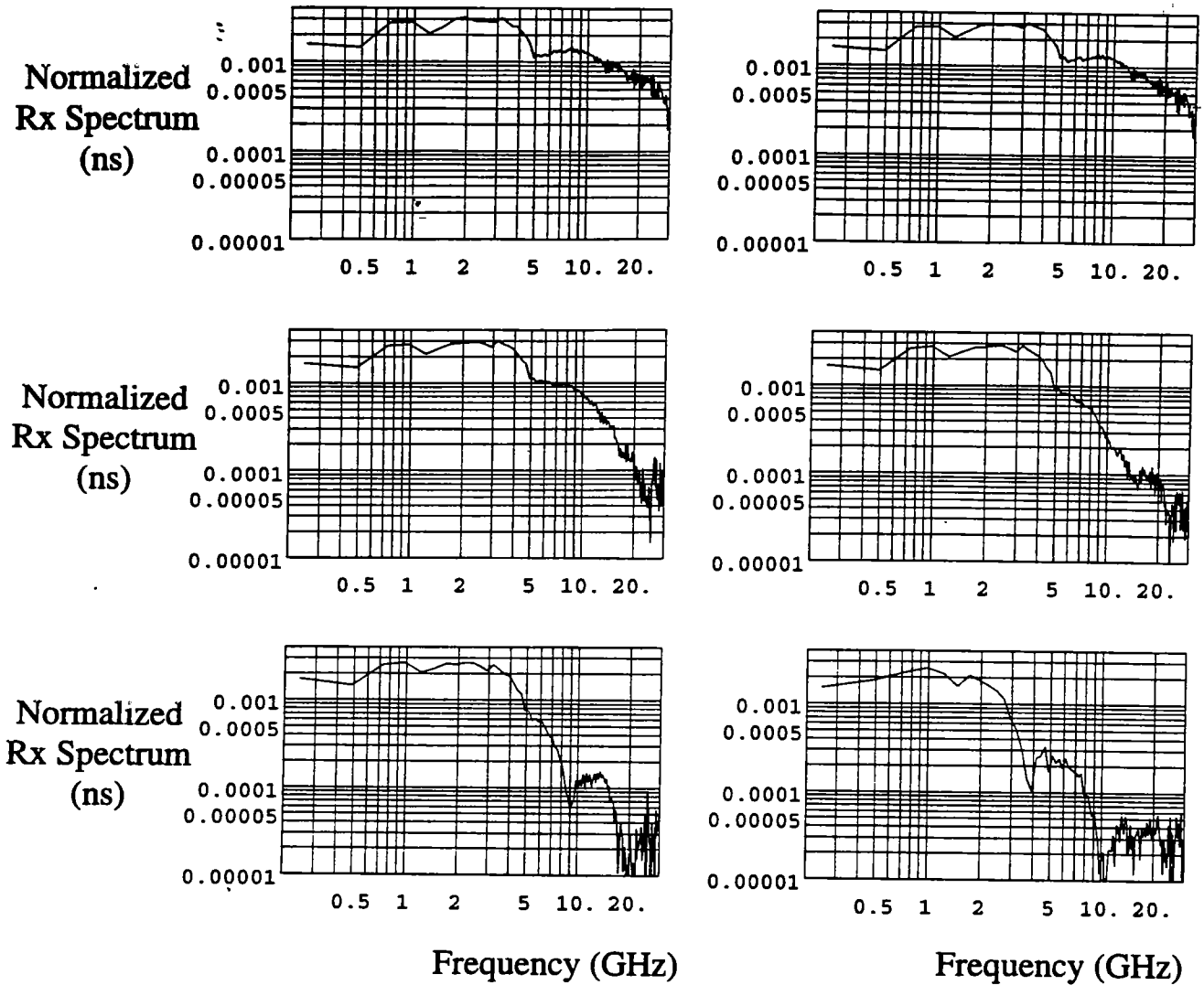

Figure 8.5 (a). E-Plane received voltage, after filtering and normalization, in the frequency domain. Waveforms are at 0, 2.5, 5, 7.5, 10, and 20 degrees off boresight.

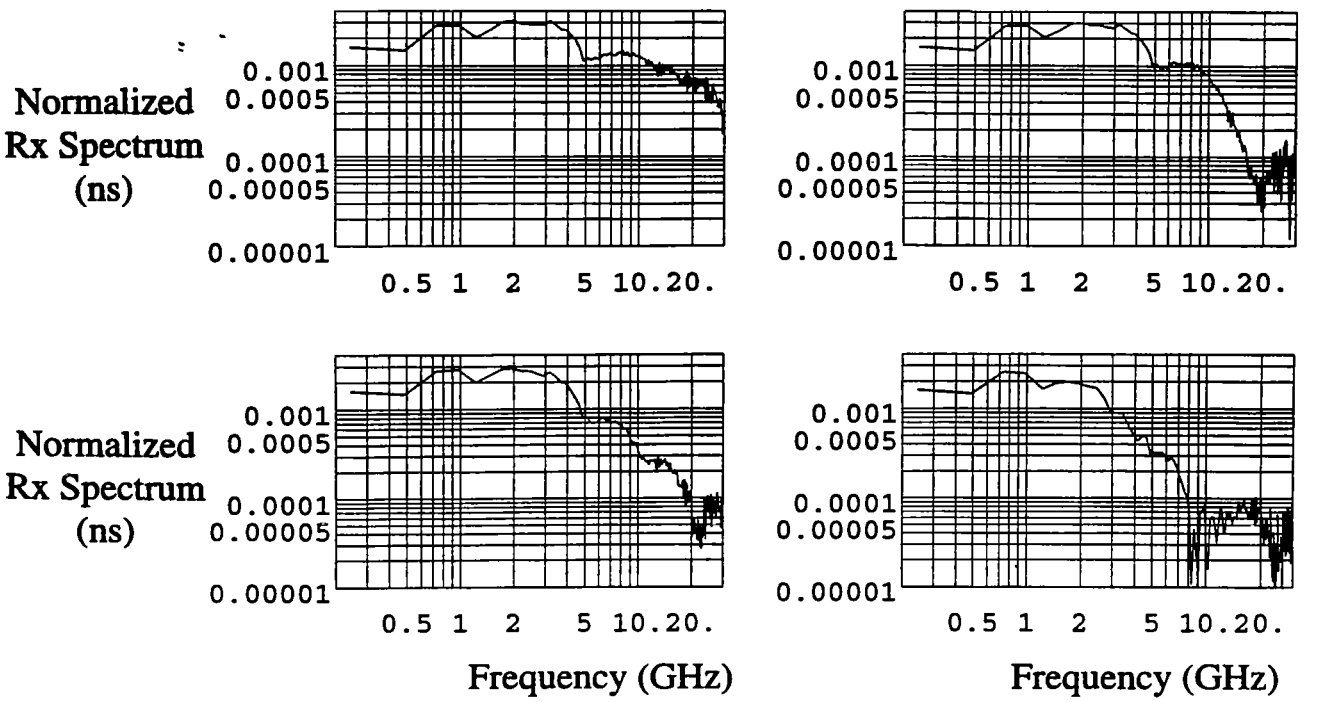

Figure 8.5 (b). H-Plane received voltage, after filtering and normalization, in the frequency domain. Waveforms are at 0, 5, 10, and 20 degrees off boresight.

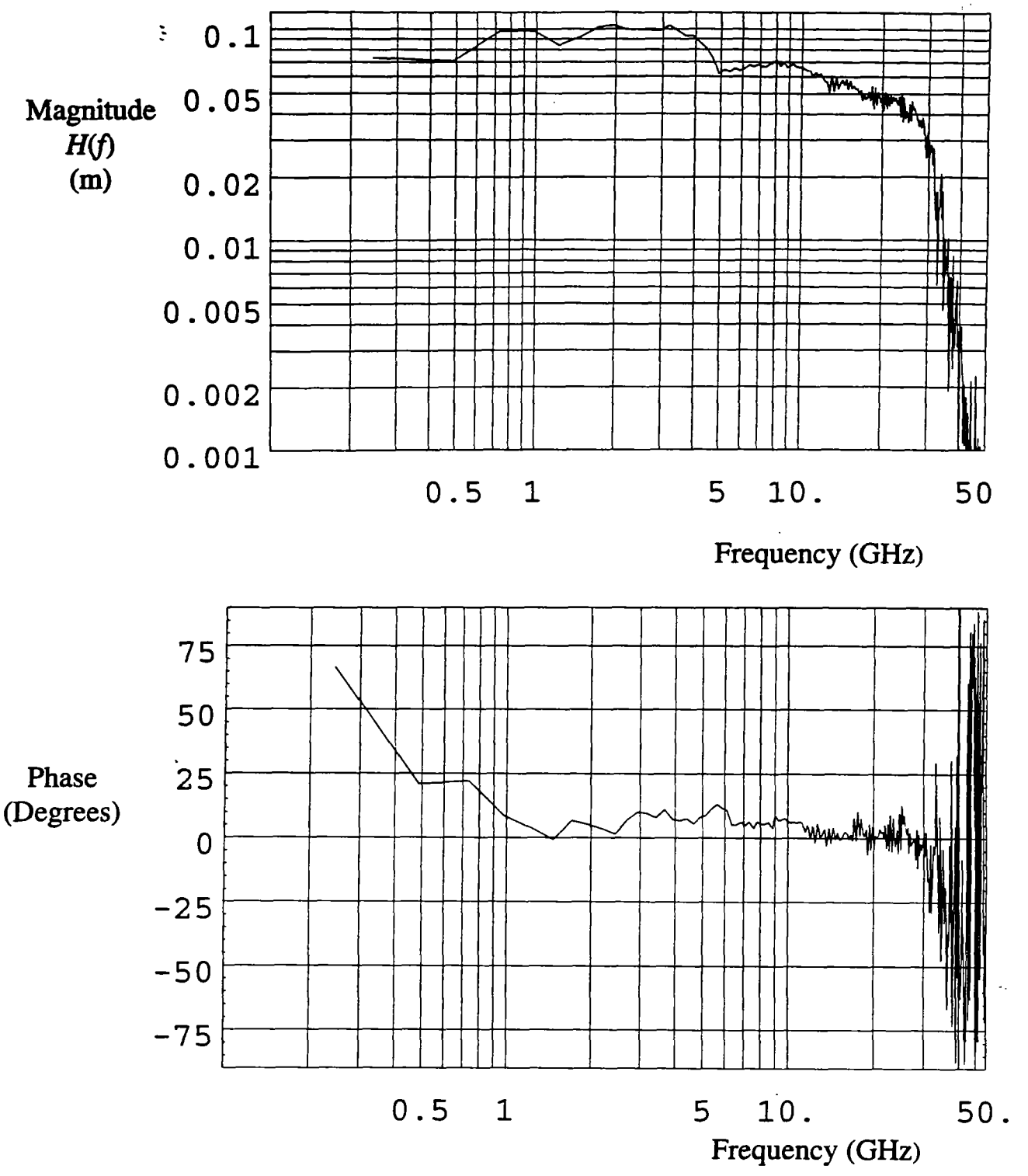

Figure 8.6. Frequency domain $H(f)$, just after taking the square root, magnitude (top) and phase (bottom). Note that the phase is essentially flat at the mid-band.

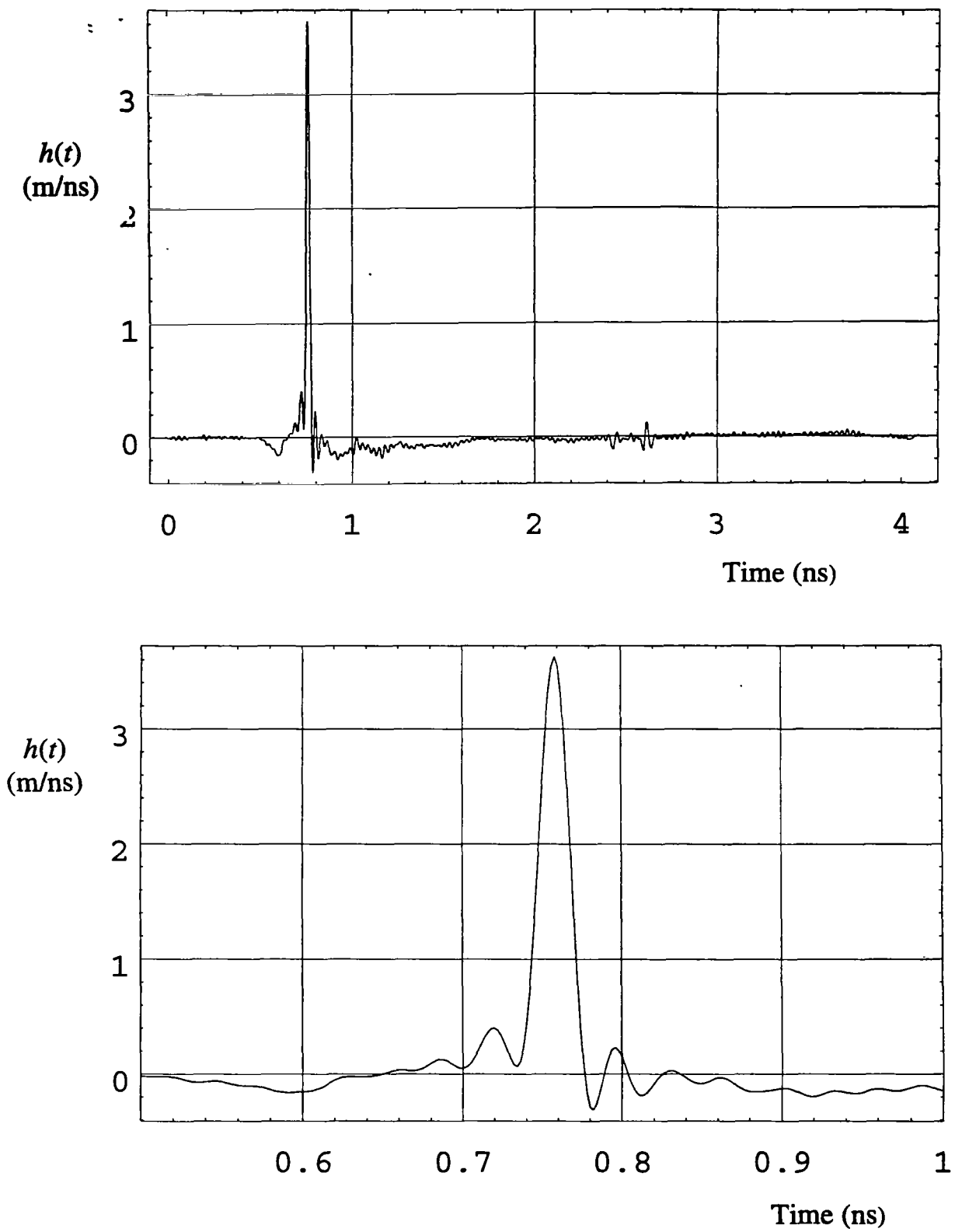

Figure 8.7 Boresight $h(t)$, entire waveform (top) and a closeup of the impulse (bottom).

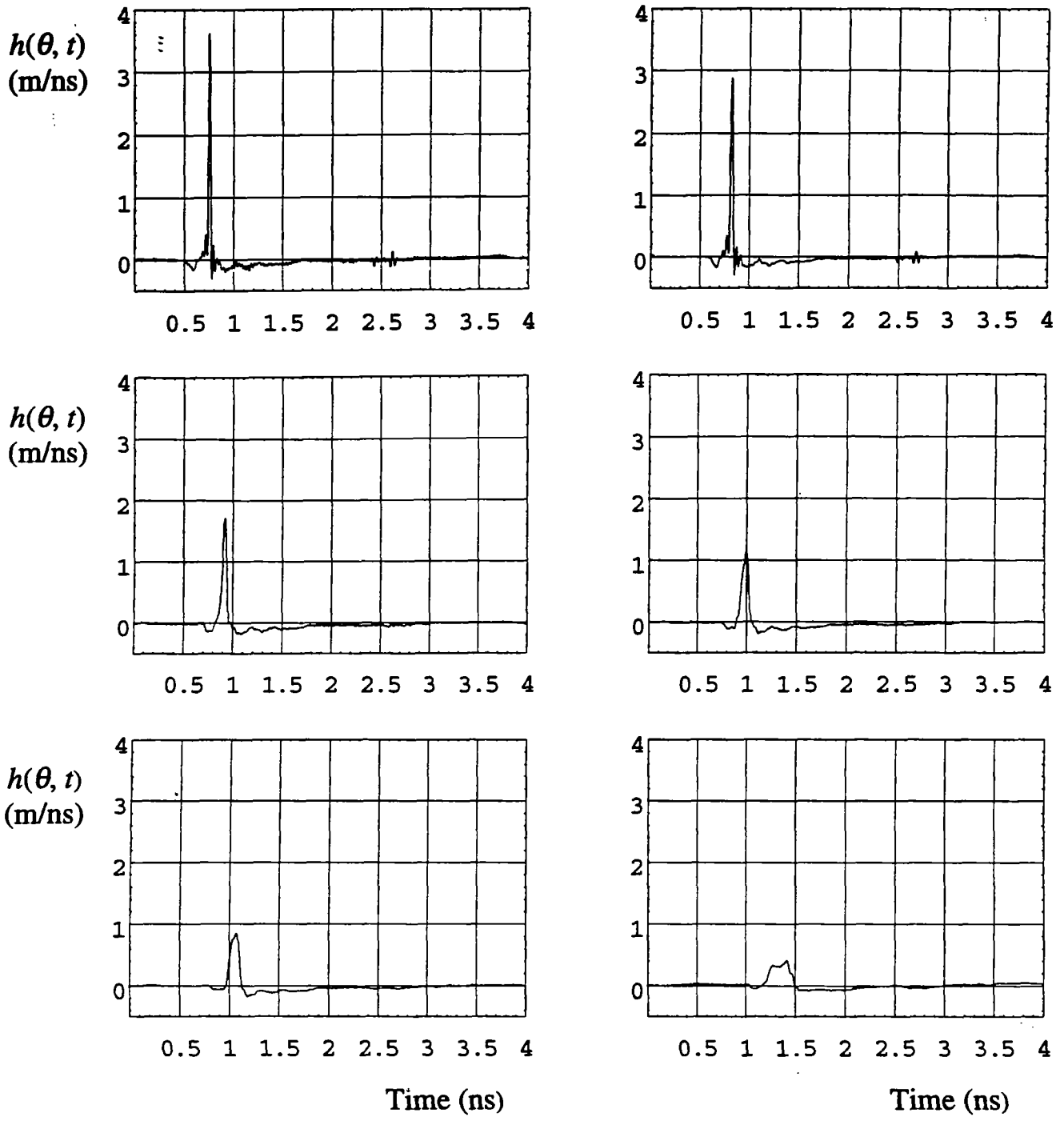

Figure 8.8(a) E-plane $h(\theta, t)$ at 0, 2.5, 5, 7.5, 10, and 20 degrees off-boresight.

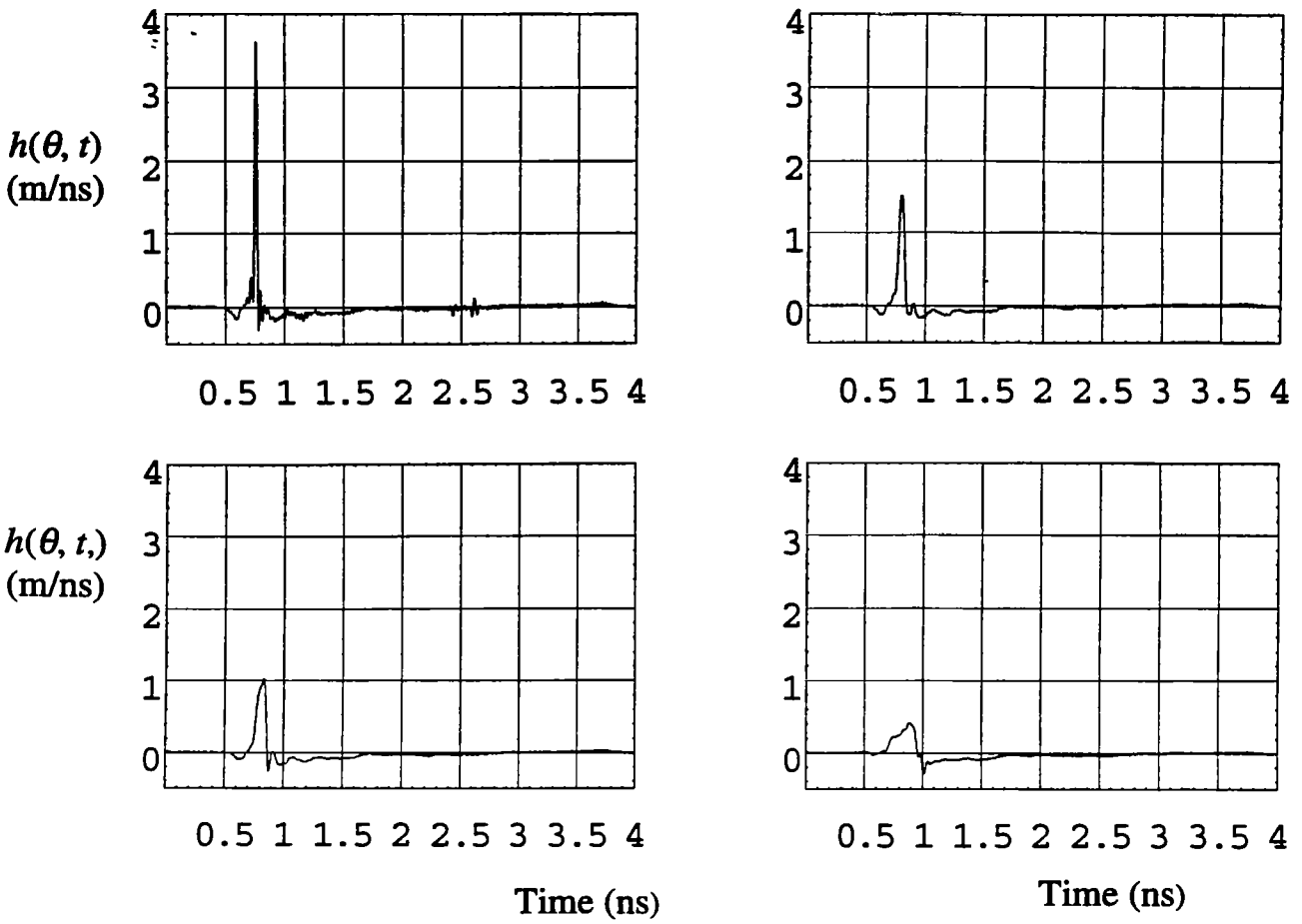

Figure 8.8(b) H-plane $h(\theta, t)$ at 0, 5, 10, and 20 degrees off-boresight.

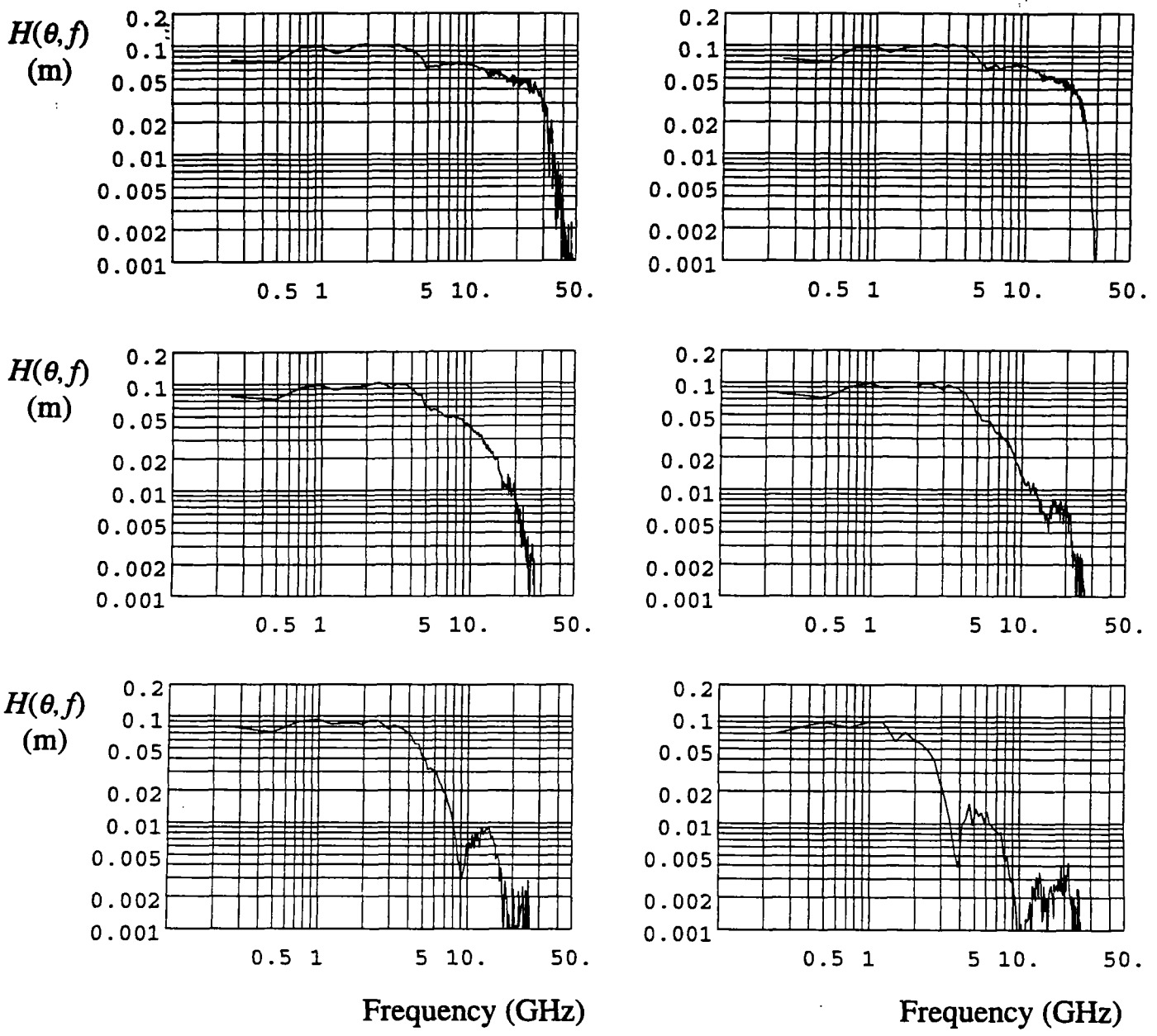

Figure 8.9(a) E-plane $H(\theta, f)$ at 0, 2.5, 5, 7.5, 10, and 20 degrees off-boresight.

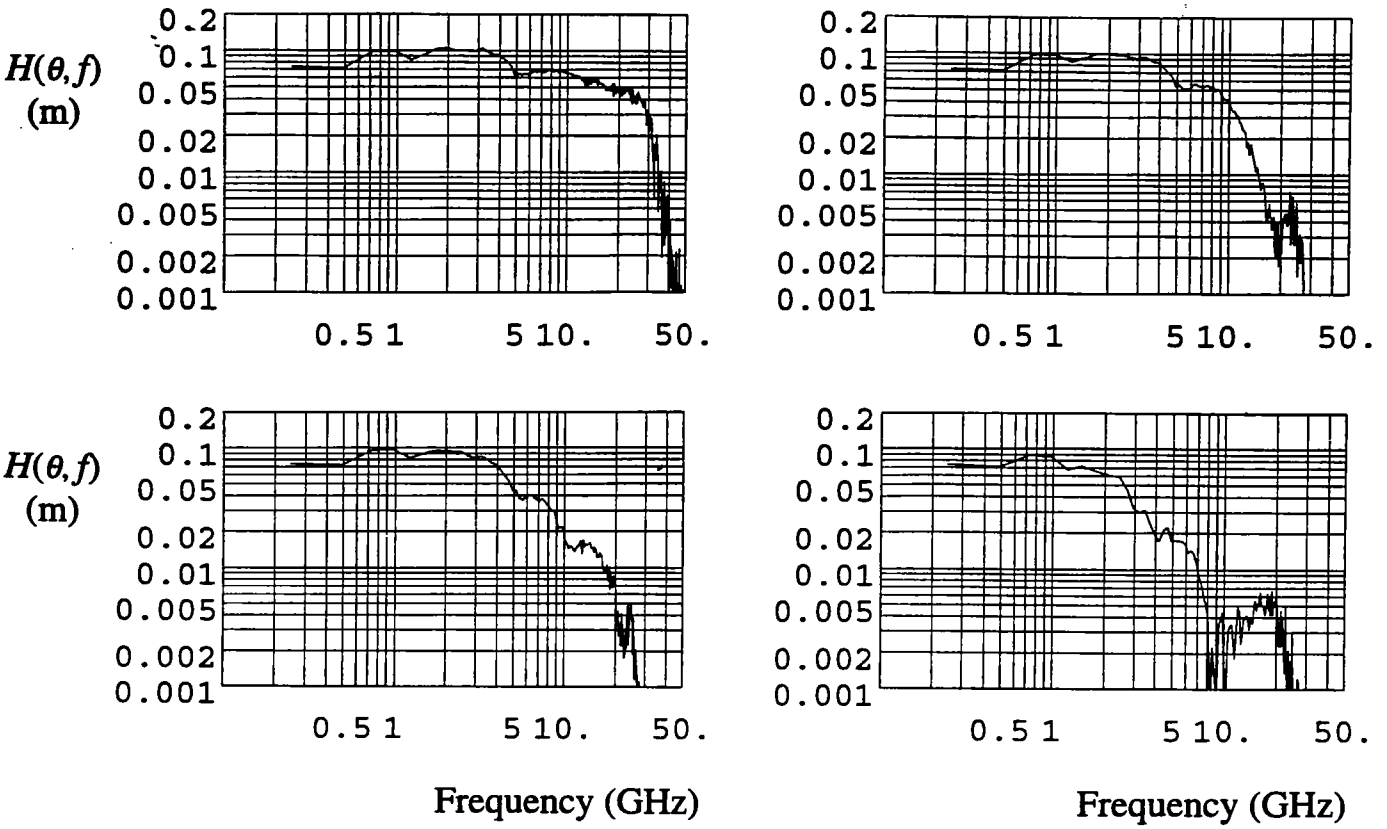

Figure 8.9(b) H-plane $H(\theta, f)$ at 0, 5, 10, and 20 degrees off-boresight.

IX. Additional Measurements and Data Interpretation for the Lens IRA

We consider here some additional calculations and measurements associated with the reflector IRA.

First, we calculate the gain pattern of the reflector IRA. As for the reflector IRA, we plot the peak magnitude of $h(\theta,t)$ in the E- and H-planes, for the six angles shown in Figures 8.8(a) and for the four angles shown in 8.8(b). The results are shown in Figure 9.1. If the beamwidth is defined as the width where the pattern is down by 0.707 from the peak (half power), then the half-beamwidth is about 4 degrees in the E-plane and 3 degrees in the H-plane. This beamwidth will occur with an ideal step-function excitation voltage.

Next, we consider a more meaningful definition of gain, as was defined in [5]. This is useful for the more practical case of a finite risetime pulser. Thus, we convolve the response of the antenna with a Gaussian of finite risetime, in this case 50 ps. This is exactly the same procedure as was described earlier in equations (5.1-5.2). The results are shown in Figure 5.2. If we define the beamwidth as angle where the pattern is down by a factor of 0.707, the half beamwidths are 7.5 degrees in both the E- and H-planes. Once again, this demonstrates that as the driving voltage becomes broader, the antenna beam also becomes more broad. For a 100 ps risetime pulser the beamwidth will be approximately twice the values for a 50 ps risetime.

Finally, we show the Time Domain Reflectometry data for the reflector IRA. The experimental setup was shown previously in Figure 5.3, and the results are shown in Figure 9.3.

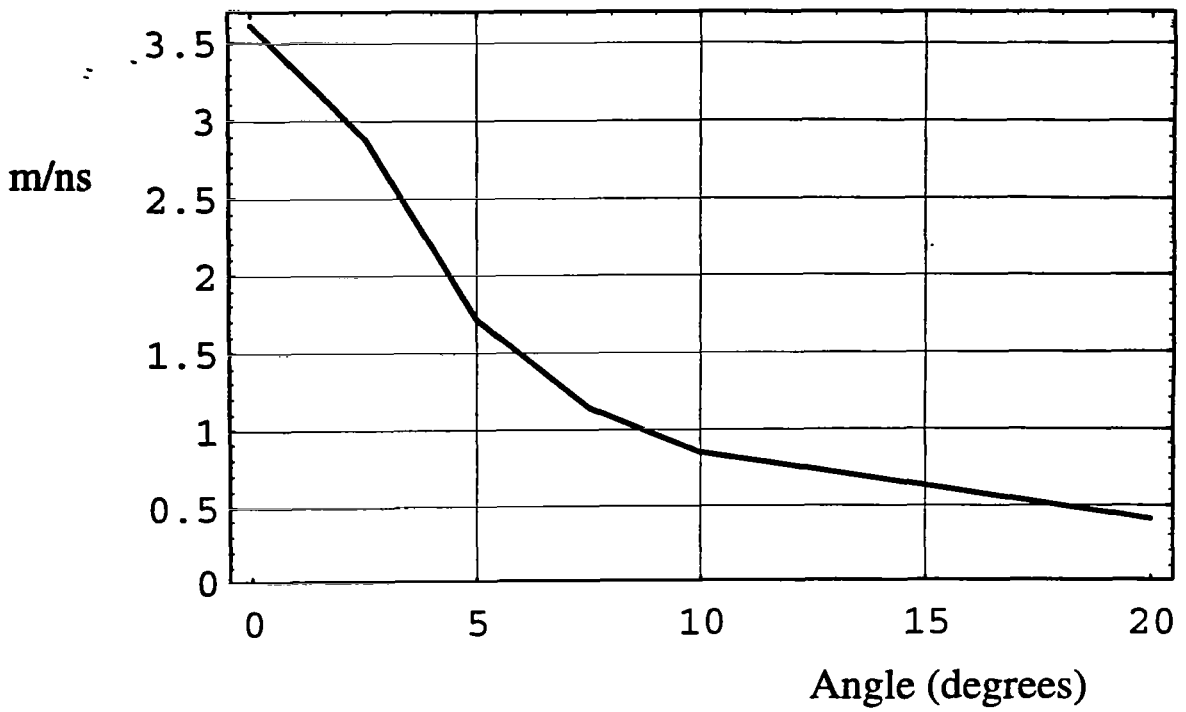

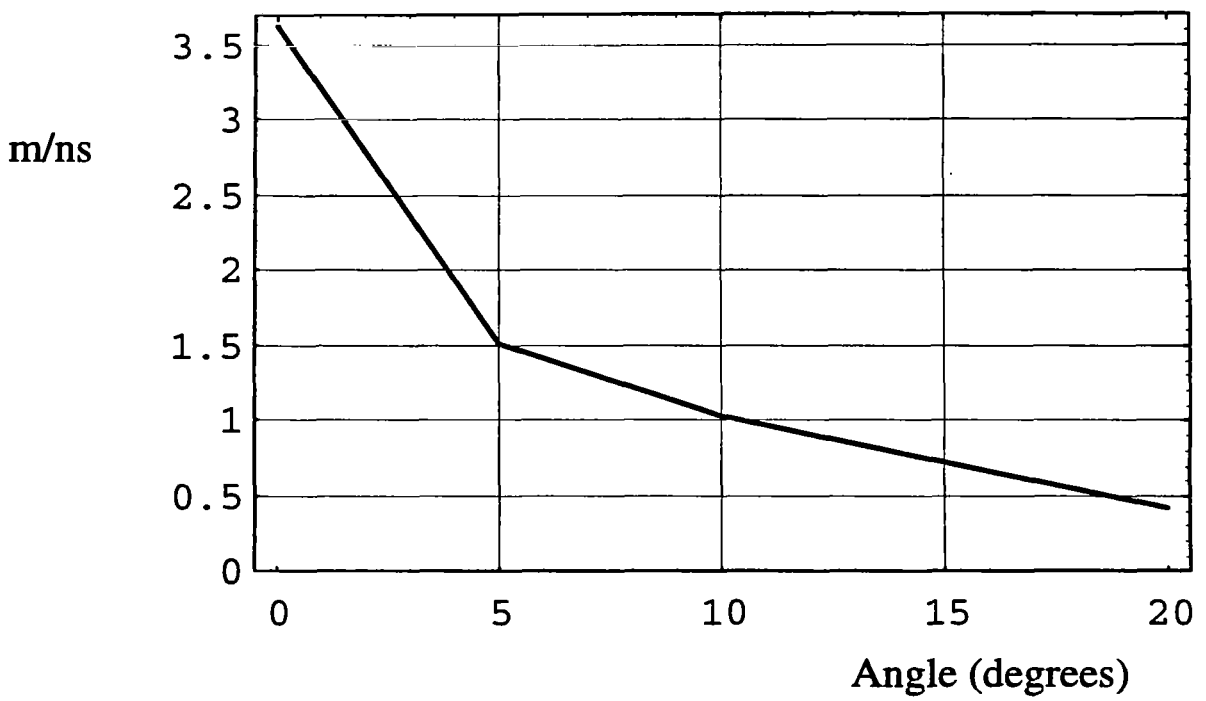

Figure 9.1. Gain of the 23 cm (9-inch) reflector IRA plotted as a function of angle off-boresight in the E-plane (top) and in the H-plane (bottom). Here gain is used in the peak $h(t)$ sense, with perfect step excitation.

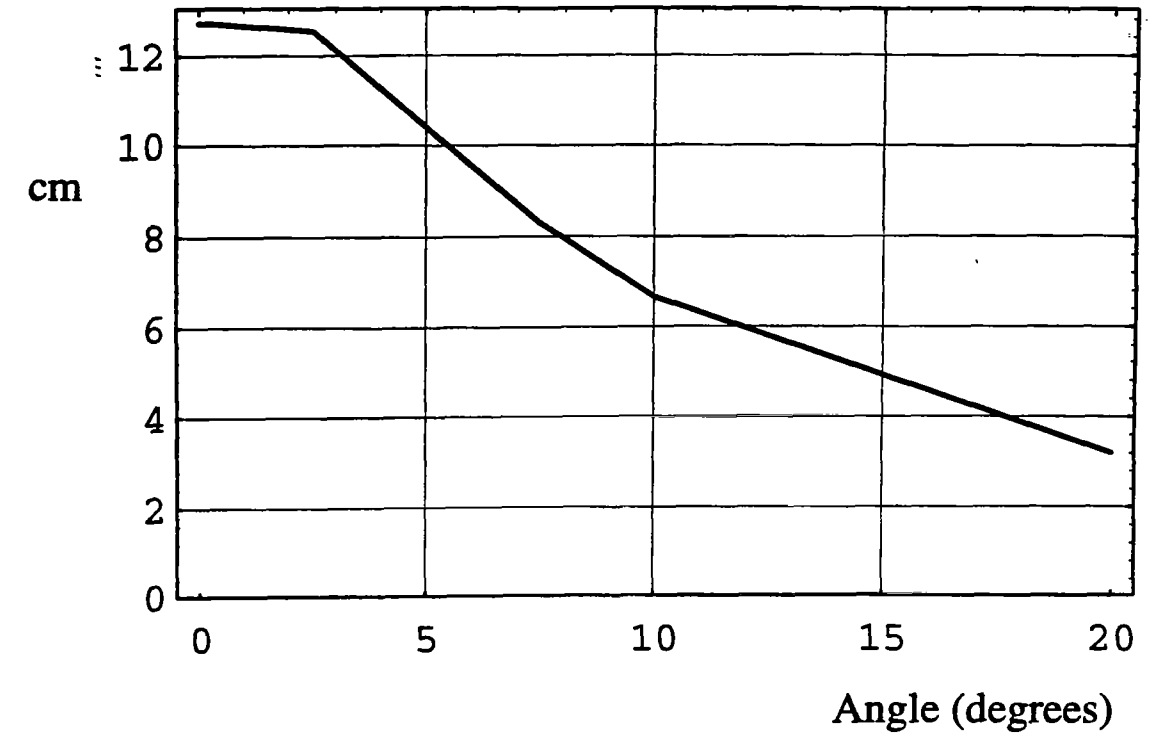

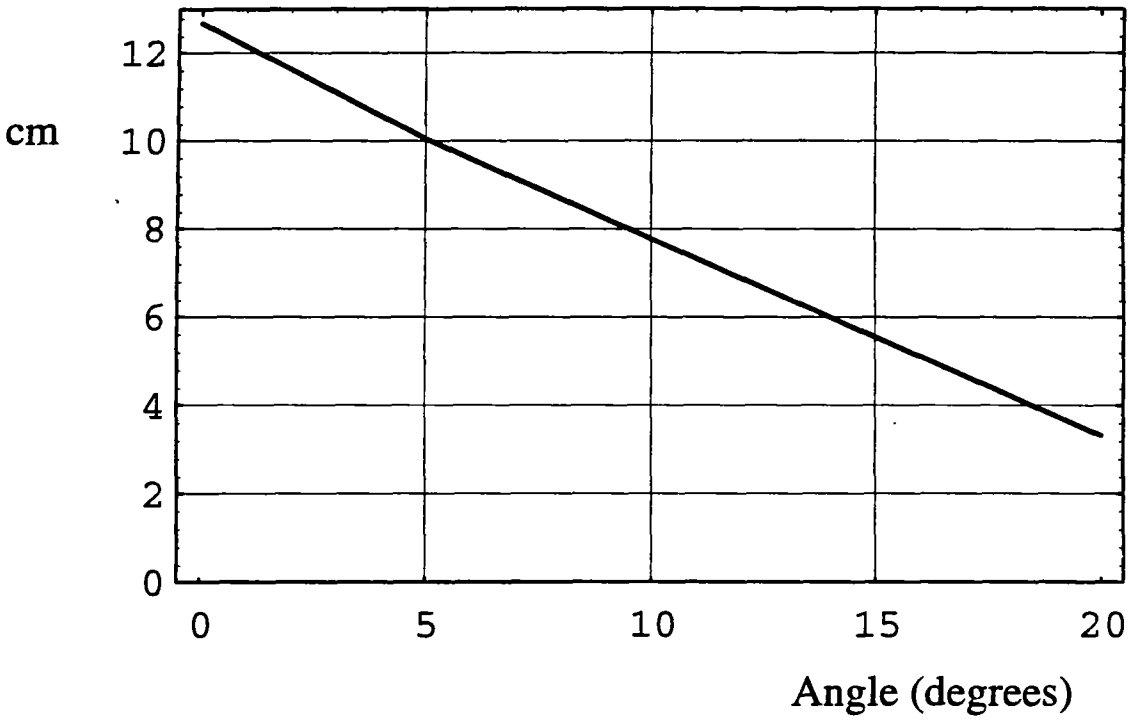

Figure 9.2. Gain of the 23 cm (9-inch) reflector IRA plotted as a function of angle off-boresight in the E-plane (top and in the H-plane (bottom). Here gain is as defined in Equation 5.1 for 50 ps risetime step excitation.

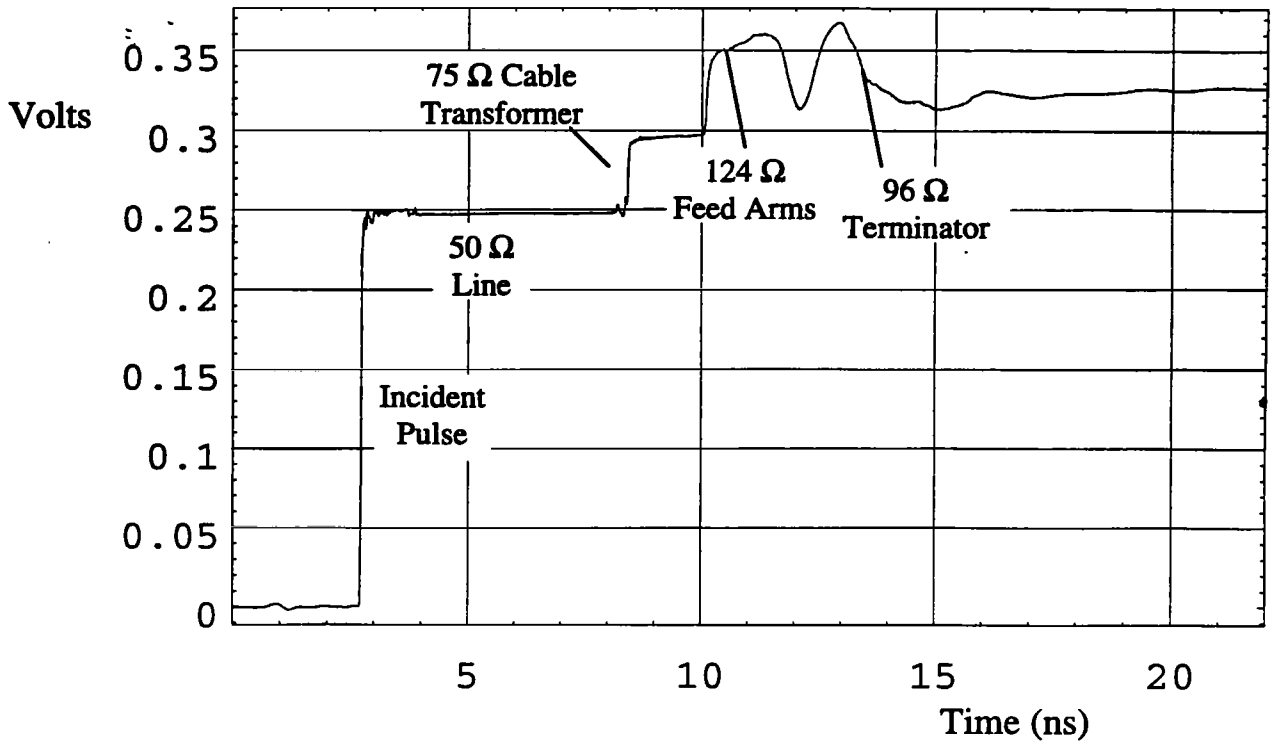

Figure 9.3. TDR of the lens IRA.

X. Conclusions

We have completed the measurements of the reflector and lens IRAs, whose design was first described in Sensor and Simulation Note 396. Our measurements showed that the design criteria in [1] were valid, and the antennas performed as expected. The area of the measured impulse was 87 % of the predicted value for the reflector IRA, and 101 % of the prediction for the lens IRA. The angular dependence of the antennas was measured, and the half-power points for both antenna types occurred approximately four degrees off-axis for step function excitation. Furthermore, we measured a FWHM of 25 ps for the reflector IRA, and 21 ps for the lens IRA. To get such fast responses, several issues were critical. First, much care was taken at the apex of both antennas. Second, the instrumentation system included a fast clean pulser (Picosecond Pulse Labs Model 4015) and a very low-noise sequential sampling digitizer (Tektronix Model 11801). Finally, all cable lengths were kept to a minimum. The measurements show that the dielectric-filled lens IRA, while heavier, gives significantly higher performance for a given aperture than the reflector IRA. The design criteria for the reflector and lens IRAs have now been validated by experimental measurements. This should allow scaling to larger and smaller sizes with confidence.

Acknowledgments

We wish to that Dr. Kwang Min of Wright Lab / MNMF for funding this work.

References

1. E. G. Farr and C. A. Frost, Development of a Reflector IRA and a Solid Dielectric Lens IRA, Part I: Design, Predictions, and Construction, Sensor and Simulation Note 396, April 1996.

2. E. G. Farr and C. A. Frost, Compact Ultra-Short Pulse Fuzing Antenna Design and Measurements, Sensor and Simulation Note 380, June 1995.

3. C. E. Baum, Configurations of TEM Feed for an IRA, Sensor and Simulation Note 327, April 1991.

4. E. G. Farr, Optimizing the Feed Impedance of Impulse Radiating Antennas, Part I: Reflector IRAs, Sensor and Simulation Note 354, January 1993.

5. E. G. Farr, C. E. Baum, and C. J. Buchenauer, Impulse Radiating Antennas, Part II, in L. Carin and L. B. Felsen (eds.) *Ultra-Wideband, Short Pulse Electromagnetics, 2*, Proceeding of the Conference held in Brooklyn NY, in October 1994, Plenum Press, 1995, pp. 159-170.